The Samapleu mafic-ultramafic intrusion and its Ni-Cu-PGE mineralization: an Eburnean (2.09 Ga) feeder dyke to the Yacouba layered complex (Man Archean craton, western Ivory Coast)

Franck Gouedji, Christian Picard, Yacouba Coulibaly, Marc-Antoine Audet, Thierry Auge, Philippe Goncalves, Jean-Louis Paquette, Naomi Ouattara

Bull. Soc. géol. France, 2014, t. 185, n° 6, pp. 393-411

The Samapleu mafic-ultramafic intrusion and its Ni-Cu-PGE mineralization: an Eburnean (2.09 Ga) feeder dyke to the Yacouba layered complex (Man Archean craton, western Ivory Coast)

FRANCK GOUEDJI[1,2,3], CHRISTIAN PICARD[1*], YACOUBA COULIBALY[2], MARC-ANTOINE AUDET[3], THIERRY AUGE[4], PHILIPPE GONCALVES[1], JEAN-LOUIS PAQUETTE[6] and NAOMI OUATTARA[5]

Key-words. – Man, Archean, Paleoproterozoic, Ivory Coast, Yacouba layered complex, Ni-Cu sulfides.

Abstract. – The Yacouba layered complex intrudes the Archean (3.5-2.7 Ga) Kenema-Man craton in the Samapleu-Yorodougou area, western Ivory Coast. In Samapleu area, the complex was recognized in drill holes at three locations: Samapleu Main (SM); Samapleu Extension 1 (E1) and Yorodougou (Yo). It comprises websterites, peridotites and gabbro-norites arranged symmetrically with mafic layers at the center and ultramafic layers at both margins. The complex is inclined at 70-80° to the SE. The thickness of individual layers varies from 2 to 60 m and the total thickness is 120 to 200 m. At the E1 site, the complex extends to depths > 500 m.

Contacts with the country rock gneiss are characterized by a hybrid zone that is a few meters thick and composed of plagioclase-orthopyroxene bearing metabasites, and locally (E1 site) a metamorphic assemblage of sapphirine-cordierite-sillimanite-spinel ± rutile. This assemblage is attributed to contact metamorphism during intrusion of the complex in the lower crust at a depth of about 25 km. Zircons in country rock gneisses and granulites, as well as in the hybrid facies, yield Archean ages of ~ 2.78 Ga, similar to ages reported in the Man craton. Rutiles in the hybrid zone give a U-Pb age of 2.09 Ga, which is interpreted as the age of contact metamorphism and emplacement of the intrusion.

The Samapleu Main and Samapleu Extension 1 sites contain Ni and Cu sulfide deposit with reserves estimated as more than 40 million tons grading 0.25% Ni and 0.22% Cu (Sama Nickel-CI, August 2013). The Ni-Cu mineralization is composed of pentlandite, chalcopyrite, pyrrhotite and rare pyrite, which is disseminated mainly in pyroxenite or occurs as subvertical and semi-massive to massive sulfide veins. The sulfide textures range from matrix ore, net-textured, droplets or breccia textures. Zones enriched in PGM, particularly Pd, are associated with the sulfides and several chromite bands are also present. These observations suggest that an immiscible sulfide liquid formed from a parental silicate liquid and percolated through the crystal pile.

The parental melt composition, determined using the Chai and Naldrett [1992] method, has a SiO_2-rich mafic composition with 53% SiO_2 and 10% MgO. This result, the presence of the hybrid zone, and the trace-element signature determined using the Bedard [1994] method, suggest a mantle-derived basaltic parental magma that had assimilated abundant continental crust.

These observations indicate that Samapleu intrusion corresponds to a magmatic conduit of the Yacouba complex as at Jinchuan (China), Voisey's bay (Canada), Kabanga (Tanzania) or Nkomati (South Africa).

Les séquences mafiques-ultramafiques de Samapleu et leur minéralisation en Ni-Cu-EGP : un dyke nourricier Eburnéen (2,09 Ga) du complexe lité Yacouba (craton archéen de Man, Côte d'Ivoire)

Mots clés. – Man, Archéen, Paléoprotérozoïque, Côte d'Ivoire, Complexe lité Yacouba, Sulfures Ni-Cu

Résumé. – Le complexe mafique-ultramafique lité Yacouba est intrusif au sein des granulites gneissiques du craton archéen Kenema-Man (3,5-2,7 Ga) dans la région de Biankouma (ouest de la Côte d'Ivoire). Dans le secteur de Samapleu-Yorodougou, ce complexe a été reconnu par sondages sur 3 sites distincts : Samapleu Main (SM) ; Samapleu Extension 1 (E1) et Yorodougou (Yo). Il comprend des horizons de webstérites, péridotites et de gabbro-norites minéralisés en sulfures de nickel (Ni) – cuivre (Cu) et en minéraux du groupe du platine (MGP). Ces horizons, d'épaisseurs variables (2 à 60 m) sont inclinés de 70 à 80° vers le SE et présentent un enracinement de plus de 500 m de profondeur sur le site E1. Ils sont disposés de manière symétrique avec les horizons ultramafiques en bordure et ceux mafiques au centre et présentent une épaisseur cumulée de 120 à 200 m. Les contacts avec l'encaissant gneissique sont marqués par une zone hybride de quelques mètres d'épaisseur, formée de métabasites à plagioclase – orthopyroxène avec localement (site E1) une paragenèse métamorphique à saphirine-cordiérite-sillimanite-spinelle +/– rutile. Ces roches sont interprétées comme le résultat d'un métamorphisme de contact lors de la mise en place de l'intrusion en base de croûte, soit à environ 25 km de profondeur. Les gneiss et granulites du socle, tout comme les faciès de la zone hybride, préservent des

1. Université de Franche-Comté (UMR 6249), 16, route de Gray, 25000 Besançon, France.
2. LGSM, UFR STRM, Université Félix Houphouët Boigny, 22 BP 582 Abidjan 22, Côte d'Ivoire.
3. Sama Nickel-CI sarl, 2 plateaux Vallons, 28 BP 1467, Abidjan 28, Côte d'Ivoire.
4. BRGM, Unité de connaissance et exploration des gîtes minéraux, 3, avenue Claude-Guillemin, BP 36009, 45060 Orléans cedex 2, France.
5. BNETD Cocody-Côte d'Ivoire, 04 BP 945, Abidjan 04, Côte d'Ivoire.
6. Laboratoire Magmas & Volcans, UMR6524 CNRS & Université B. Pascal, 5 Rue Kessler, 63038 Clermont-Ferrand cedex, France.
*Corresponding author : christian.picard@univ-fcomte.fr
Manuscript deposited on January 25, 2014; accepted on July 7, 2014

âges Archéen (~2.78 Ga, U-Pb sur zircon) similaires aux âges classiquement cités dans le craton de Man. Des cristaux de rutile observés dans la zone hybride révèlent un âge U-Pb de 2.09 Ga qui est interprété comme l'âge du métamorphisme de contact et donc de la mise en place de l'intrusion.

La minéralisation en Ni-Cu est composée de pentlandite, chalcopyrite, pyrrhotite, rarement pyrite. Elle apparaît disséminée essentiellement dans la pyroxénite avec des veines sulfurées subverticales semi-massives à massives qui forment un chevelu ouvert vers le haut. La texture des sulfures varie de matricielle, en filets, en gouttelettes, ou brèchique. Des MGP riches en palladium (Pd) sont associés aux sulfures et plusieurs bandelettes de chromite sont également présentes. Ces observations suggèrent un liquide sulfuré immiscible formé à partir du liquide silicaté initial consécutivement à la saturation en soufre du système. Ce liquide aurait ensuite percolé au travers des silicates cristallisés.

La composition du liquide parent déterminé à l'aide de la méthode de Chai et Naldrett [1992] révèle une composition mafique avec 53 % SiO_2 et 10 % MgO. Cette composition et la signature en éléments traces déterminées selon la méthode de Bédard [1994], suggèrent un magma issu de la fusion partielle du manteau et qui a assimilé une abondante proportion de croûte continentale lors de sa mise en place en base de croûte.

Ces observations indiquent que l'intrusion de Samapleu correspond très vraisemblablement à un conduit magmatique du complexe Yacouba à l'image de Jinchuan (Chine), Voisey's bay (Canada), Kabanga (Tanzanie), ou Nkomati (Afrique du Sud).

INTRODUCTION

Magmatic nickel and copper sulfides, together with platinum group elements (PGE), occur worldwide within mafic or ultramafic sequences: in komatiitic flows or intrusions (Raglan and Thompson in Canada; Kambalda in Australia); high magnesium intrusions (Norilsk in Russia, Kabanga in Tanzania, Nkomati in South Africa, Jinchuan in China, Voisey's bay in Labrador); layered complexes (Bushveld in South Africa, Sudbury in Canada), as summarized by Naldrett [2004], Jebrak and Marcoux [2008]; Arndt and Ganino [2010]. Except for Norilsk, which is Triassic, all these deposits are located in Archean to Paleoproterozoic provinces within or adjacent to Precambrian cratons.

There are no active base metal mines in the entire West African region, and only a few Ni-Co and Cr + PGE occurrences are known. One example is the Guelb el Azib layered complex in Mauritania [Berger *et al.,* 2013]. Another, known as the Samapleu Ni-Cu-PGE deposit [Ouattara, 1998], is in the Archean Man craton in Côte d'Ivoire (Ivory Coast).

Nickel and copper sulfide mineralization was first identified in Côte d'Ivoire in 1976 in the vicinity of Yorodougou village by SODEMI during a stream and soil sampling program (fig. 1a-b). The prospect, later named the Samapleu deposit, was confirmed with 40 cores drilled by SODEMI over a period spanning from 1980 to 1997. This drilling showed that the Ni-Cu-PGE mineralization was hosted within peridotite-pyroxenite-gabbro and gabbro-norite cumulate units. Ouattara [1998] interpreted the entire sequence as a layered intrusion of lower Proterozoic (2.6 Ga) age.

From 1996, the project remained dormant, and it was only in 2009 that exploration work by Sama Resources Inc resumed. Local and regional geological mapping, together with geophysical surveys (ground magnetic, induced polarisation, InfiniTEM, airborne magnetic, radiometric and electromagnetic) and more than 30.000 m of drilling in 245 boreholes confirmed the existence of the mafic-ultramafic sequence described by Ouattara [1998]. The Samapleu Main (SM) mineralized zone was defined by Sama Nickel CI in 2010. In August 2010, the Samapleu Extension 1 (E1) was discovered 0.5 km north of SM (fig. 2) and later the same year, the Yorodougou occurrence (Yo) was discovered 5 km east of SM. Exploration is presently ongoing and three new mineralised sites were recently discovered along a 25 km long Samapleu-Bounta corridor (fig. 2), the Cr enriched Gossan and Glata savane occurrences (Sama Nickel-CI, 2012), and additional Ni-Cu sulfides at the Yepleu site (Sama Nickel-CI, 2013) which is located 18 kilometers SW of the Samapleu deposits. It is highly probable that all these occurrences are part of a single magmatic complex, which Sama Nickel-CI named the Yacouba layered complex.

This article describes general geology of the complex and more specifically the petrology, geochemistry and mineralogy of the Samapleu intrusions and their Ni-Cu-Cr-PGE mineralization. The geodynamic environment is discussed, and a hypothesis for the origin of the intrusions and the associated mineralization is developed.

REGIONAL GEOLOGY

The Yacouba layered complex in the Yorodougou-Samapleu-Bounta area

The Yacouba mafic and ultramafic layered complex is located within the Archean Kenema-Man craton at the eastern margin of the West Africa shield (fig. 1a). Camil [1984], Kouamelan *et al.* [1997] and Pitra *et al.* [2010] described the Man craton as a granulitic terrane mainly composed of 3.05 Ga aged orthopyroxene-rich tonalitic gneiss and 2.8 Ga charnockites, all affected by Liberian (2.9 to 2.7 Ga) metamorphism.

The study area is located ~ 50 kilometers north of the Man-Danané fault (fig 1b), near the villages of Yorodougou, Samapleu and Bounta (fig. 2), in exploration regions jointly owned by "Sama Nickel-CI" and "Société pour le Développement Minier de la Côte d'Ivoire (SODEMI)". The area is 100 kilometres west of the Sassandra fault, which separates the Archean domain from the Proterozoic Birrimian sequences. As in most of the Man craton, the area contains Opx-rich tonalites, felsic granulites, quartzites and garnet + quartz-rich pyroxenites. Mafic-ultramafic sequences are noted on the SODEMI geological map of Côte d'Ivoire (1972).

The ultramafic to mafic Yacouba layered complex (fig. 2) extends along a 25 km long corridor from Bounta to Samapleu-Yorodougou. It is composed of layered gabbro,

gabbro-norite, diorite, anorthosite and a magnetite-rich unit, forming dismembered and stretched assemblages that are several meters to around 200 meters thick. The sequence also contains massive chromite layers, identified at surface in more than six locations along the Samapleu-Bounta corridor. Nickel-copper sulfide-rich sequences are present at the Samapleu (this paper) and Yepleu (fig. 2-3).

Structural geology

The study area is generally hilly with a challenging topography (fig. 2). Variation in elevation can exceed 500 m locally with very steep slopes particularly around Bounta. The Samapleu-Yorodougou sector, located at the base of the mountainous ridge, has a more gentle topography with low rolling hills and flatter plateaux and savannah type vegetation. Intense weathering produces alteration profiles locally exceeding 40 m. The geological maps reproduced in figures 2 and 3 summarize structural and geological information from relatively poor surface exposures and knowledge from geophysical surveys and drill holes (fig. 2-3).

The Archean country rocks in the Samapleu and Santa areas display a NE-SW regional foliation steeply dipping 70° to 90° towards SE or NW; in the Bounta area, the foliation is sub-horizontal to slightly inclined. The magnetite rich unit which forms a marker horizon, shows thin, folded and dismembered layers whose S0-S1 structures vary from 020° to 080° in the Santa area, 030° to 105° south of Bounta and 040 to 340° NE of Bounta. These data suggest that the complex was deformed by a regional dome and basin pattern, as pictured by the distribution of the lithologies (fig. 2). In the Yorodougou area, the mafic and ultramafic sequences are generally parallel to the regional foliation.

The E1 intrusion extends for more than 2 km at the surface and varies from 50 m to 200 m in thickness (fig. 3a, b – 4a, b). It has a NE-SW strike and dips at 70°-80° to the SE. Drill holes intercepted the E1 intrusion down to a depth of at least 500 m. The ENE-WSW oriented Yorodougou occurrence is 1.5 km long at surface and dips at 70°-80° toward the SE (fig. 3a). Based on the surface geomorphology, the Samapleu section appears to form a fold hinge with a subvertical axis and the axial plane running parallel to the regional foliation. Such a fold would be responsible for the apparent inverted polarity between the three sites (fig. 3b).

Structural studies based on the regional mapping and drill holes data suggest that the Samapleu-Yorodougou area was affected by ductile deformation. The oldest recognisable event produced a set of NE-SW oriented sinistral faults that crosscut the fold hinge and affects the E1 and SM intrusions. At the SM intrusion, a NW-SE inverse fault dipping 40° to 50° to the SW has divided the deposit into two distinct compartments (fig 3b). Later vertical N-S oriented faults, parallel to the Sassandra fault, and a dextral NW-SE fault, cut the

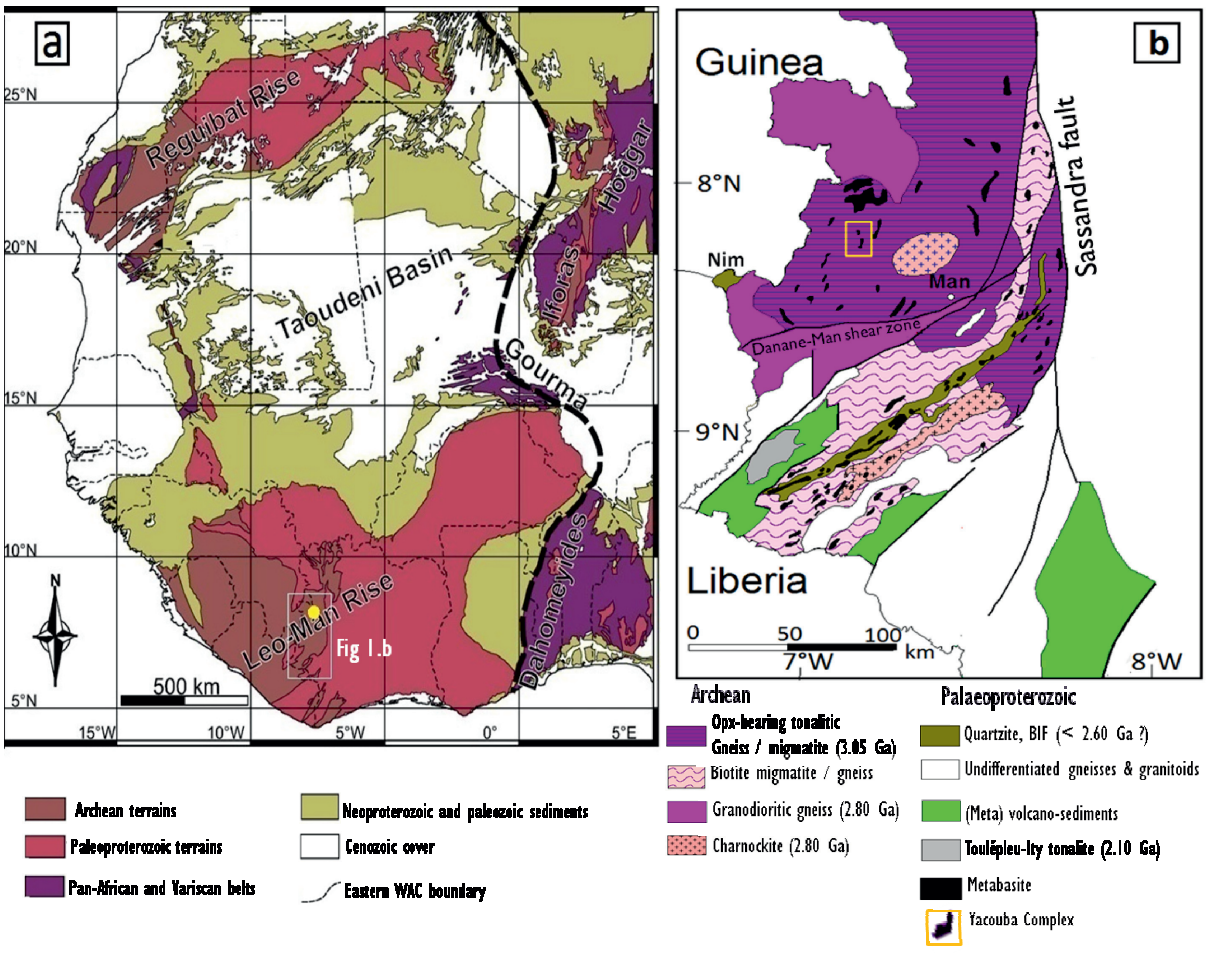

FIG. 1. – Schematic geological map. A: West African shield [Berger *et al.*, 2013]; b: Man craton in western Côte d'Ivoire [Pitra *et al.*, 2010]. Figure 1b window shows the Sipilou-Biankouma area and the Yacouba layered complex as it is currently known.

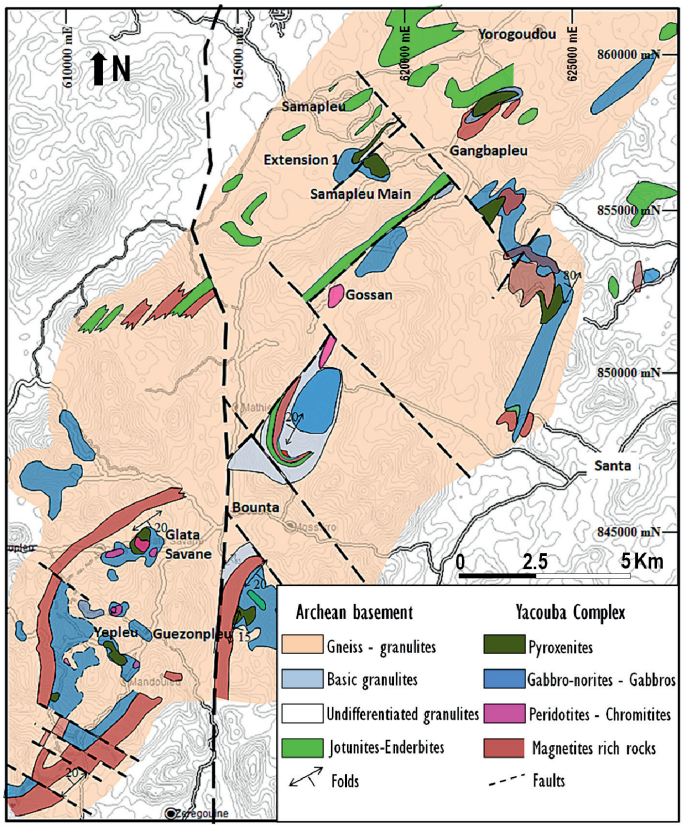

FIG. 2. – The Yacouba layered complex members including: Samapleu mafic and ultramafic facies near Yorodougou - Samapleu - Gangbapleu and Bounta villages in the Biankouma region. Samapleu Extension 1 = E1;

earlier structures (fig. 2). These structures have similar directions to those observed farther east and south in Birimian group assemblages [Coulibaly *et al.*, 2012].

SAMAPLEU MAFIC AND ULTRAMAFIC SEQUENCES

Lithostratigraphy and petrology

Petrological and mineralogical studies of the Samapleu mafic and ultramafic sequences were performed on two representative boreholes; SM24-661614 (azimuth of 135°, dip 50°) for the E1 sequence and SM44-450250b (azimuth of 225°, dip 50°) for the SM sequence. The two sequences are similar and show a succession of mafic and ultramafic facies: gabbro-norite, norite, pyroxenite, and peridotite. A sapphirine rich facies, the hybrid zone, is present in the E1 site at the contact between the mafic-ultramafic sequence and the Archean gneiss (fig. 4a and b) [Gouedji, 2014].

– **Peridotites** are mainly finely banded/sheared lherzolite composed of olivine (> 70%, $Fo_{76\ to\ 90}$) with amphibole (pargasite and tschermackite, 15-20%), enstatite, bronzite and diopside (less than 15%) and minor amounts of hercynite, magnesio-chromite and sulfides [fig. 5a]. Dunite, restricted to near the contact with Archean gneissic host, is composed of olivine, secondary magnetite and minor orthopyroxene. Generally well rounded, the olivine may show undulating extinctions and deformation kinks, evidence of high-temperature, post-magmatic deformation [Pronost, 2005]. The olivine is partly altered (3-5%) to lizardite (RAMAN spectrometry, Ecole nationale supérieure de Lyon.

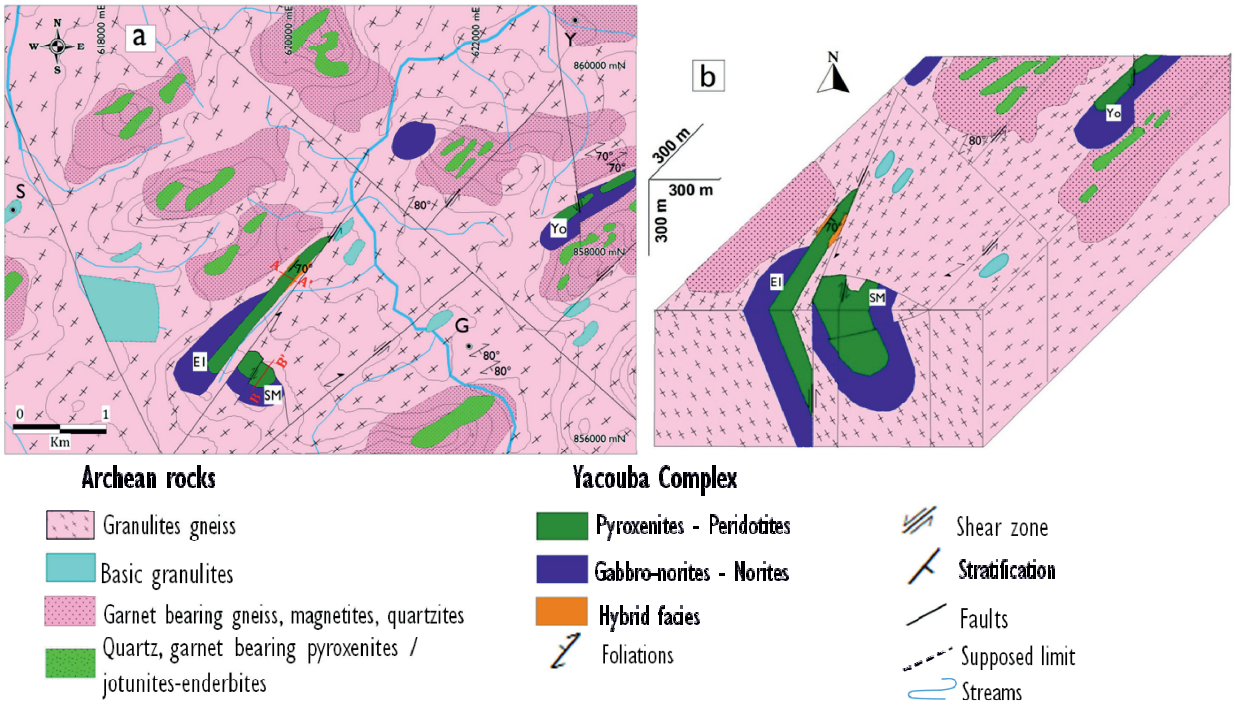

FIG. 3. – The Yacouba layered complex members including: Samapleu mafic-ultramafic sequences in the Samapleu-Yorodougou area, together with gneissic granulite and quartzite country rock. a: schematic geological map; b: block diagram. Samapleu Extension 1 = E1; Samapleu Main = SM; Yorodougou occurrence = Yo; Samapleu = S; Gangbapleu = G; Yorodougou = Y.

– **Pyroxenites** are the most abundant ultramafic rock (fig. 4a-b). Their transition from peridotite to pyroxenite is characterised by the gradual decrease in olivine content and increase in pyroxene. The pyroxenites are websterites divided olivine, plagioclase and spinel-rich varieties (tab. I; fig. 5b).

– **Gabbro-norites and norites** (tab. I; fig. 5c) form a thin level in the core of Extension 1 sequence with plagioclase cumulates and relatively important sequences in the south part of Extension 1 and around Samapleu main Sequence. At the difference of the pyroxenites, they are poorly mineralised with less than 5% sulfides. Contacts with ultramafic and mafic lithologies are generally gradual over several centimeters.

– Finally, **the 2 to 15 m thick hybrid zone** is mainly located at the footwall contact with the gneissic country rock. This zone, which can be easily confused with a norite, contains an assemblage of pyroxene (bronzite), plagioclase (labradorite) and biotite with local sapphirine, cordierite, sillimanite, hercynite, grenat ± rutile assemblage (fig. 5d) which indicate high-pressure, high-temperature metamorphism conditions (around 7-8 kbar and 700 to 950°C, Gouedji [2014]). Xenoliths of granulite are often seen together with this metamorphic assemblage.

All mafic and ultramafic units are cut by calcite-chlorite-muscovite-quartz and feldspar veins suggesting late hydrothermal activity.

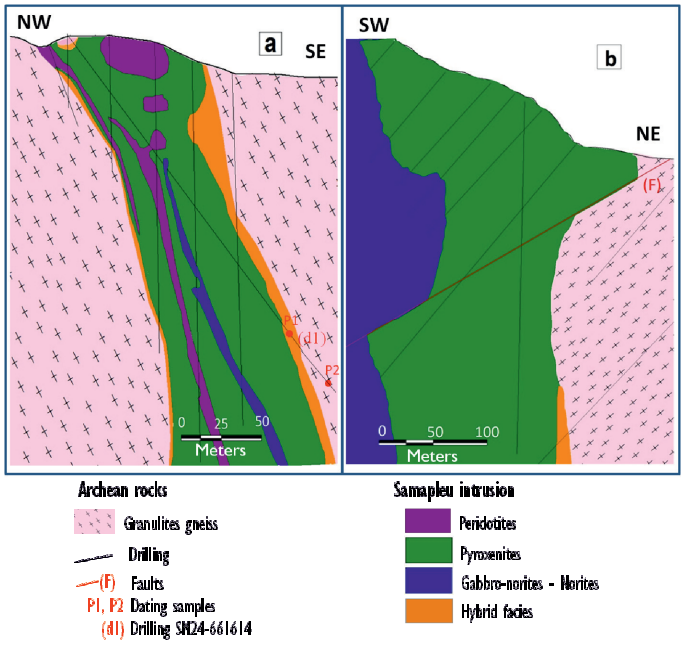

FIG. 4. – Cross-section showing Samapleu mafic-ultramafic sequences from borehole data. a: Line AA' Samapleu Extension 1 (fig. 3a); b: Line BB' Samapleu Main (fig. 3a).

Geochemistry

A total of 35 samples (tab. II-IV), six from gneiss or granulite units, 23 from barren peridotite, pyroxenite and gabbro-norite, and six from the hybrid zone, were collected from borehole SM-24661614 in E1. Four additional samples were collected from the hybrid zone in boreholes SM24-628688 and SM24-645670.

Samples were analysed for major and trace elements using optical spectrometry (ICP-OES) and ICP-MS at the CRPG of Vandoeuvre, Nancy, France, using techniques described by Carignan et *al.* [2001].

Several geochemical signatures are observed in the intrusion (fig. 6). The granulites contain 65-70% SiO_2, 14-17%, Al_2O_3 and 1-6% MgO. They are strongly enriched in light

TABLE I. – Lithologies of the Samapleu intrusions

Sequences	Lithologies	Mineralogies	Descriptions, remarks
Peridotites	Lherzolite (fig. 5a)	70% olivine (Fo_{76} to $_{90}$ – Ø = 1 to 3 mm); 15-20% amphibole (pargasite and tschermackite); < 15% pyroxene (enstatite, bronzite and diopside); Minor amounts of hercynite, magnetite, magnesio-chromite and Ni-Cu sulfides.	Olivine phases partially serpentinized (3 to 5% lizardite); can show strait contacts and undulating extinctions as well as deformation kinks.
	Dunite	90% olivine with less of 5% magnetite derived from olivine during serpentinisation; Minor amounts of orthopyroxene.	Dunite, located near the contact with Archean gneissic host.
Pyroxenites	Olivine-rich websterite	10 to 20% olivine; > 60% pyroxene (bronzite and less amount of diopside); 10-15% pargasite; 5% spinel and 5% sulfides	Similar characteristics than the lherzolite with the difference, which is the olivine content. Olivine-rich websterite is only observed near the surface in contact with the lherzolite. Pyroxenes display a poecilitic texture. Pargasite is xenomorph.
	Websterite sensu-stricto (fig. 5b)	70% bronzite, 10-15% diopside, 15-20% green amphibole (pargasite) <10% spinels (hercynite, picotite, chromite, magnetite)	Spinels form exsolution within large pyroxene crystals. Websterite is the main host for the sulfide mineralization.
	Plagioclase-rich websterite	Same mineralogical composition that websterite with 10 to 15% plagioclase (An_{90-95}) - 5 to 10% tschermackite	Xenomorph to sub-automorph plagioclase minerals are in post-cumulus phase between bronzite, diopside and tschermackite crystals.
	Spinel-rich websterite	Same mineralogical composition that olivine-rich websterite with 30 to 40% of spinel (chrome-spinel-picotite-pleonaste)	Spinels are found in interstitial position between olivine and pyroxene minerals.
Mafic Unit	Gabbro-norite (fig. 5c)	>50% plagioclase (An_{80-84}); 35-40% bronzite; 15% diopside; 5-10% amphibole (pargasite and tschermackite); < 5% sulfides.	Spinels and olivine are absent in gabbro-norite. These mafic units are poor in sulfides.
	Norite	Same mineralogical composition that gabbro-norite; rare Cpx	Same that gabbro-norite

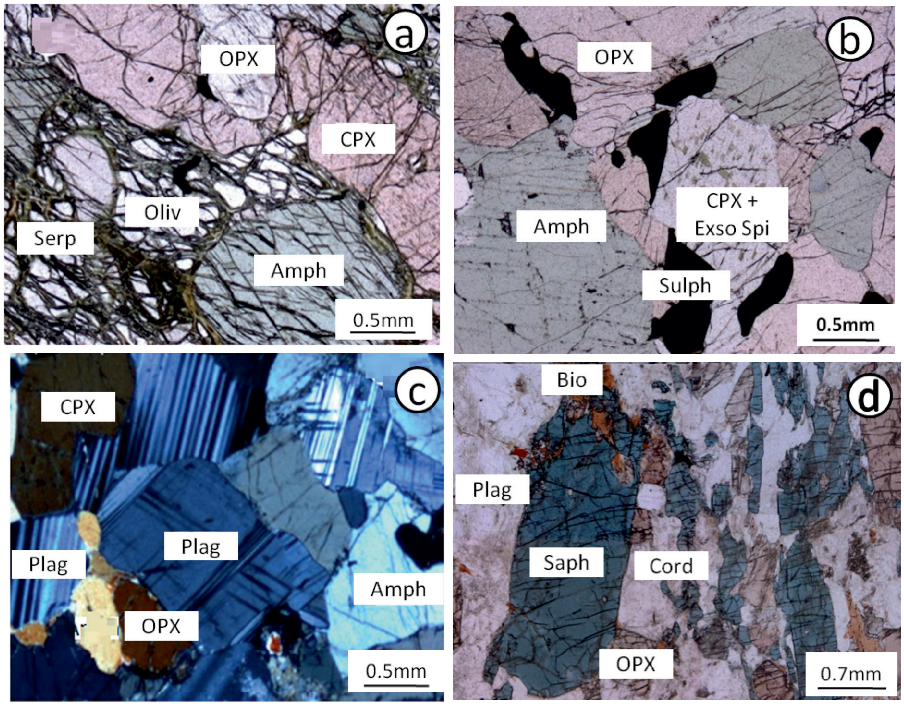

FIG. 5. – Photomicrographs of various members of the Samapleu intrusion. A: partially serpentinized lherzolite; b: pyroxenite; c: gabbro-norite; d: hybrid zone with sapphirine. Bio = biotite; Plag = plagioclase; Saph = sapphirine ; Serp = serpentine; Amph = amphibole ; Oliv = olivine ; Cord = cordierite ; CPX = clinopyroxene ; OPX = orthopyroxène; Sulph = sulfide; Exso Spin = exsolution spinel

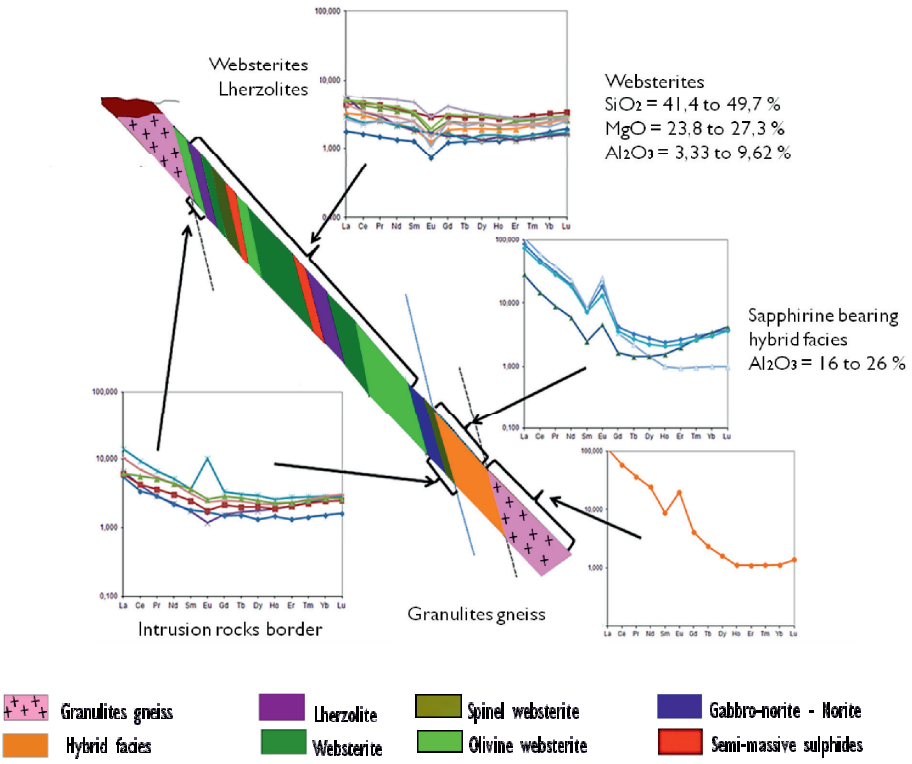

FIG. 6. – E1: SM24-661614 drilling log and proposed stratigraphic succession and associated rare earth geochemical signatures.

rare earth elements (LREE – 100 time chondrite values with (La/Sm)n = 9.3-13.6) but display a fairly flat spectrum for the heavy rare earth elements (HREE; (Dy/Yb)n=1.2-1.4).

The peridotites contain 38-39% SiO_2, 2-3% Al_2O_3 and 31-33% MgO. Pyroxenites contain 41-51% SiO_2, 3-12% Al_2O_3 and 18-29% MgO; and gabbro-norites 46-48% SiO_2, 19-20% Al_2O_3 and 10-12% MgO (tab. III). REE concentrations (fig. 6) are two to eight times chondrite values. Features such as the high MgO and low Al_2O_3, TiO_2 and REE of the ultramafic rocks and the high Al_2O_3 of the gabbro-norites reflect the cumulus nature of the rocks.

Rocks from the hybrid zone contain 39-56% SiO_2, 3-22% MgO and 10-33% Al_2O_3. These values, together with those of the REE (tab. IV), are intermediate between the mafic-ultramafic rocks of the intrusion and the enclosing granulites, suggesting mingling of magma with the host rocks, or contamination of the magma with these rocks, or a combination of both processes.

In figure 7, major elements are plotted against MgO, which decreases from lherzolites to websterites, and finally to gabbro-norites. Three different trends are observed. The first, from lherzolites to olivine websterites, displays increases of SiO_2, Al_2O_3 and CaO and are collinear with the composition of olivine containing 42-44% MgO (or Fo_{80-83}). This suggests that these rocks contained a variable proportion of cumulus olivine. TiO_2, K_2O and Na_2O also increase, but their contents vary greatly and remain very low (0.3, 0.3 and 0.1% respectively). The second trend from olivine websterites to plagioclase websterites displays a more important increase of SiO_2, while Al_2O_3, CaO, FeO and TiO_2 decrease probably due to accumulation of pyroxene and plagioclase that crystallized from more evolved liquids.

TABLE II. – Major (wt%) and trace (ppm) elements geochemistry for the granulitic gneiss at the Samapleu E1 Zone (SM24-661614 Drill-core). Data from CRPG Nancy, France.

Lithologies	Granulite gneiss					
Drilling holes	SM24-645670	SM24-661614				
Samples	SM24 (3)/50.6	SM24/56.2	SM24/66.5	SM24/318	SM24/320.1	SM24/329.5
Depth (m)	50.6	56.2	66.5	318	320.1	329.5
SiO_2	65.85	70.21	64.97	68.35	68.86	70.18
TiO_2	0.50	0.45	0.50	0.43	0.46	0.42
Al_2O_3	16.99	15.71	14.50	16.09	16.50	14.49
Fe_2O_3	4.94	2.98	7.75	3.13	3.55	3.18
MnO	0.06	0.02	0.09	0.04	0.04	0.04
MgO	2.85	1.52	6.11	1.42	1.37	1.43
CaO	2.73	2.88	2.07	3.96	3.68	3.11
Na_2O	4.67	5.10	3.62	4.79	5.00	4.30
K_2O	0.76	1.17	0.43	0.73	0.94	1.21
P_2O_5	0.09	0.04	0.04	0.07	0.06	0.07
LOI	-0.03	0.57	0.31	0.77	0.43	1.40
Total	99.39	100.65	100.39	99.79	100.89	99.84
Ni	21.13	ld	ld	29.75	ld	12.87
Co	11.79	9.13	18.70	10.58	11.19	8.51
Cr	56.21	28.34	49.71	33.25	32.38	33.06
Cu	56.00	170.40	30.50	211.70	164.30	91.04
Zn	45.07	36.55	106.20	44.97	32.54	40.38
Ba	444.80	523.60	379.70	599.60	644.30	915.10
Rb	4.57	6.52	0.50	1.88	1.34	9.09
Sr	420.40	423.00	291.50	558.50	497.70	431.10
Pb	7.77	11.47	6.67	9.34	8.55	10.72
Hf	4.41	3.73	4.60	2.44	3.26	2.38
Nb	4.91	3.22	6.13	1.79	2.27	2.51
Ta	0.26	0.15	0.39	0.08	0.11	0.10
Th	2.84	0.20	1.25	0.05	0.18	0.35
U	0.23	0.13	0.24	0.08	0.10	0.14
V	46.53	37.75	73.03	39.73	39.07	34.09
Y	6.57	0.81	10.47	1.72	1.95	2.78
Zr	192.50	157.10	191.20	107.40	137.70	106.20
La	34.17	41.59	31.94	26.97	35.59	30.71
Ce	54.67	63.06	47.44	37.38	51.42	46.48
Nd	17.74	17.76	13.96	11.46	14.72	14.03
Sm	2.73	1.95	2.16	1.34	1.65	1.84
Eu	0.95	1.05	0.86	1.15	1.16	1.07
Gd	2.17	0.86	2.49	0.84	0.91	1.16
Tb	0.28	0.07	0.39	0.09	0.10	0.12
Dy	1.42	0.24	2.06	0.41	0.43	0.57
Ho	0.23	0.03	0.36	0.06	0.07	0.10
Er	0.59	0.11	0.96	0.18	0.21	0.26
Tm	0.08	0.02	0.14	0.03	0.03	0.04
Yb	0.56	0.13	0.98	0.19	0.22	0.27
Lu	0.09	0.03	0.16	0.04	0.04	0.05

*Note: ld = detected limit

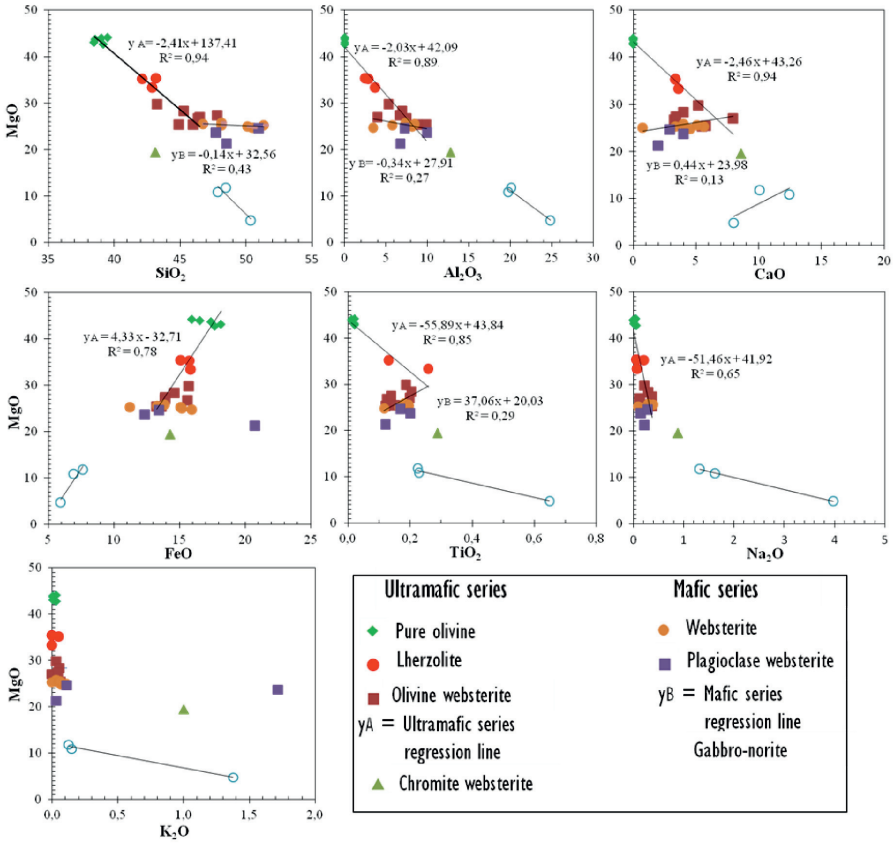

FIG. 7. – Major element diagrams (SiO_2, Al_2O_3, CaO, Na_2O, FeO, TiO_2 and K_2O) with MgO of Samapleu sequence cumulates. R^2 = distribution coefficient.

TABLE III. – Major (wt%) and trace (ppm) elements geochemical data for the mafic and ultramafic cumulates at the Samapleu E1 zone (SM24-661614 drill-core). Data from CRPG Nancy, France.

	Lherzolite			Olivine websterite								Websterite						Chromite websterite	Plagioclase websterite			Gabbro-norite	
Samples	SM24 /83	SM24 /173.8	SM24 /182	SM24 /208.5	SM24 /108.2	SM24 /239	SM24 /76.7	SM24 /67.8	SM24 /118.4	SM24 /197.6	SM24 /217.5	SM24 /139	SM24 /156.5	SM24 /67.4	SM24 /97.8	SM24 /186	SM24 /274.8	SM24 /271	SM24 / 257.4	SM24 / 260.3	SM24 /266.3	SM24 /251	SM24 / 254.5
Depth (m)	-83	-173.8	-182	-208.5	-108.2	-239	-76.7	-67.8	-118.4	-197.6	-217.5	-139	-156.5	-67.4	-97.8	-186	-275	-271	-257.4	-260.3	-266	-251	-254.5
SiO_2	38.62	38.16	38.94	45.14	43.63	43.73	45.46	42.87	41.46	44.99	46.31	46.47	50.84	48.60	46.91	43.47	48.68	40.64	46.05	45.66	49.67	46.67	47.39
TiO_2	0.23	0.11	0.12	0.12	0.20	0.12	0.19	0.13	0.18	0.15	0.13	0.16	0.19	0.11	0.18	0.18	0.16	0.27	0.12	0.19	0.16	0.22	0.22
Al_2O_3	3.34	2.22	2.65	7.27	6.68	9.62	3.90	3.33	5.13	8.64	6.47	7.38	5.72	3.33	7.17	7.86	7.90	12.02	6.42	9.48	7.05	19.20	19.66
Fe_2O_3	15.87	14.82	16.21	16.90	15.68	14.75	15.11	19.10	16.75	14.42	15.01	16.22	12.35	17.06	15.05	13.75	16.39	14.97	21.90	13.14	14.59	7.50	8.31
MnO	0.26	0.21	0.24	0.20	0.19	0.19	0.32	0.32	0.20	0.19	0.19	0.22	0.24	0.34	0.20	0.15	0.25	0.15	0.28	0.17	0.22	0.13	0.13
MgO	30.02	31.27	32.52	26.03	27.33	24.67	26.37	27.03	28.53	24.87	26.52	24.34	25.01	23.79	25.14	23.78	24.25	18.33	20.16	22.68	23.97	10.59	11.53
CaO	3.24	3.00	3.10	3.18	3.86	5.33	7.77	4.17	4.96	5.67	3.32	3.25	5.57	4.39	3.93	4.77	0.75	8.11	1.88	3.82	2.87	12.13	9.87
Na_2O	0.07	0.06	0.20	0.12	0.28	0.36	0.14	0.34	0.21	0.31	0.36	0.10	0.30	0.27	0.29	0.37	0.21	0.84	0.22	0.15	0.28	1.58	1.29
K_2O	ld	ld	0.05	0.01	0.05	0.06	ld	0.08	0.03	0.04	0.05	ld	0.05	0.07	0.03	0.06	0.11	0.29	0.03	1.65	0.11	0.15	0.12
P_2O_5	ld	ld	ld	ld	ld	ld	ld	ld	Ld	ld	ld	ld	ld	ld	ld	ld	0.05	0.08	ld	Ld	ld	ld	ld
LOI	6.48	7.89	4.65	-0.22	-0.08	1.14	1.19	1.03	0.59	0.40	0.25	-0.20	-0.03	2.25	0.05	3.64	-0.07	0.96	0.33	1.02	0.43	1.03	0.80
Total	98.12	97.74	98.67	98.75	97.81	99.95	100.45	98.38	98.04	99.68	98.60	97.94	100.23	100.20	98.95	98.02	98.68	96.66	97.38	97.95	99.35	99.21	99.32
Ni	2554	1919	2094	1776	1649	2009	1356	1378	2661	1299	1325	1612	592.60	3020	1108	1288	1464	1148	2727	1029	1057	252.4	279.60
Co	173.10	139.80	168.10	131.70	134.80	143.00	114.70	119.80	181.20	119.00	124.30	113.10	63.75	155.70	108.90	112.50	105.60	105.80	181.00	94.30	79.90	42.19	49.55
Cr	6890	7241	6927	9600	9428	5401	4125	7147	3603	6278	3481	8648	4092	5171	540.70	8689	6980	20037	5390	6776	3414	695.6	756.90
Cu	510.40	333.00	233.60	688.50	284.90	651.40	648.80	582.40	940.90	369.10	519.10	530.00	75.95	1954.0	976.10	949.20	1006	820.00	2355	1227	1004	46.75	87.75
Zn	128.50	263.40	236.20	161.80	217.40	111.20	164.10	173.90	73.55	117.50	93.97	205.80	97.73	129.90	60.72	213.00	257.20	169.20	241.90	170.20	100	54.84	59.46
Ba	4.21	7.53	14.08	1.75	11.25	3.40	15.05	20.02	6.74	3.82	4.60	10.49	7.81	21.10	6.96	9.90	985.60	147.20	36.69	1166	149	81.36	235.60
Rb	ld	0.94	1.88	ld	1.10	1.02	ld	1.56	0.37	0.46	0.60	0.71	0.54	1.17	0.57	1.59	7.59	4.89	0.85	102.30	3.02	4.26	1.40
Sr	6.71	10.26	16.55	4.02	17.14	7.33	34.31	17.55	14.81	8.98	8.12	7.49	24.43	13.67	7.73	14.03	30.27	13.38	51.02	23.03	27.35	388.8	433.60
Pb	0.93	25.48	23.03	ld	18.36	ld	57.27	1.82	1.14	1.24	5.87	ld	1.71	6.73	52.87	49.16	37.81	1.78	1.24	0.94	35.84	4.88	6.00
Hf	0.15	0.23	0.16	0.15	0.23	0.17	0.33	0.43	0.25	0.27	0.19	0.14	0.23	0.20	0.34	0.36	0.22	0.42	0.17	0.36	0.51	0.20	0.15
Nb	0.00	0.00	0.20	0.18	0.00	0.45	0.34	0.58	0.30	0.39	0.53	0.11	0.33	0.54	0.39	0.33	1.03	0.72	ld	0.58	0.50	0.37	0.37
Ta	ld	ld	0.05	0.02	ld	0.07	0.16	0.08	0.04	0.08	0.05	0.02	0.03	0.08	0.04	0.04	0.19	0.08	0.02	0.07	0.09	0.02	0.02
Th	ld	ld	0.34	ld	ld	ld	0.05	0.57	0.08	0.04	0.03	ld	ld	0.39	0.13	0.33	0.08	0.62	0.05	0.22	0.18	ld	ld
U	ld	ld	0.09	ld	ld	ld	ld	0.17	ld	ld	ld	ld	ld	0.10	0.03	0.11	ld	0.20	ld	0.07	0.06	ld	ld
V	100.70	68.50	79.42	127.90	140.60	98.00	81.39	91.60	84.64	107.10	91.16	132.50	120.00	78.47	68.84	136.00	124.90	197.40	160.70	134.20	109	118.00	106.90
Y	3.41	2.80	2.77	2.07	3.54	3.09	4.74	3.22	4.38	4.48	3.15	2.34	4.29	3.96	3.48	3.81	3.09	4.43	2.52	4.43	3.69	5.15	4.35
Zr	2.36	6.75	7.22	4.75	7.12	5.00	10.73	15.52	9.27	8.40	6.56	3.68	6.94	7.06	10.41	12.86	8.66	15.23	4.55	12.81	18.33	5.42	3.47
La	0.10	0.71	1.37	0.43	0.65	0.63	1.45	1.48	1.22	1.04	0.79	0.24	0.69	1.51	1.06	1.24	1.63	3.42	0.93	2.24	2.54	1.04	1.12
Ce	0.55	1.51	2.15	1.04	1.42	1.69	3.51	2.69	3.00	2.87	1.91	0.80	2.24	3.60	2.19	2.63	2.64	5.99	1.72	6.43	4.50	2.18	1.95
Nd	0.99	1.01	1.04	0.64	1.09	1.04	2.38	1.45	1.90	1.78	1.09	0.67	1.50	2.06	1.35	1.65	1.07	2.46	0.78	3.04	2.09	1.59	1.18
Sm	0.39	0.31	0.28	0.20	0.39	0.30	0.71	0.38	0.52	0.51	0.30	0.21	0.41	0.56	0.38	0.49	0.27	0.56	0.19	0.65	0.48	0.49	0.38
Eu	0.12	0.09	0.10	0.04	0.06	0.13	0.17	0.10	0.11	0.17	0.07	0.09	0.24	0.15	0.09	0.10	0.07	0.59	0.08	0.16	0.14	0.29	0.20
Gd	0.54	0.34	0.31	0.25	0.50	0.39	0.83	0.44	0.64	0.60	0.38	0.27	0.54	0.59	0.47	0.50	0.32	0.69	0.26	0.68	0.51	0.67	0.56
Tb	0.09	0.05	0.06	0.05	0.08	0.07	0.13	0.08	0.11	0.11	0.07	0.05	0.10	0.10	0.09	0.09	0.06	0.11	0.05	0.12	0.09	0.12	0.10
Dy	0.62	0.40	0.34	0.33	0.60	0.48	0.80	0.51	0.73	0.72	0.49	0.36	0.68	0.64	0.58	0.59	0.45	0.75	0.35	0.74	0.57	0.83	0.73
Ho	0.13	0.09	0.08	0.07	0.12	0.10	0.16	0.11	0.16	0.15	0.11	0.08	0.15	0.13	0.13	0.12	0.11	0.15	0.08	0.16	0.12	0.18	0.16
Er	0.37	0.24	0.22	0.23	0.38	0.32	0.45	0.35	0.43	0.45	0.32	0.25	0.47	0.38	0.36	0.40	0.34	0.46	0.28	0.45	0.39	0.52	0.47
Tm	0.06	0.04	0.03	0.04	0.05	0.05	0.07	0.05	0.07	0.07	0.06	0.04	0.08	0.06	0.06	0.06	0.06	0.07	0.06	0.07	0.07	0.08	0.07
Yb	0.38	0.27	0.25	0.29	0.34	0.37	0.45	0.40	0.47	0.53	0.40	0.33	0.54	0.44	0.41	0.45	0.44	0.47	0.46	0.49	0.47	0.57	0.49
Lu	0.06	0.04	0.04	0.05	0.06	0.06	0.07	0.06	0.08	0.08	0.07	0.06	0.09	0.07	0.07	0.07	0.07	0.07	0.08	0.08	0.08	0.09	0.08

*Note: (1) ld = detected limit; (2); nd = not determined

TABLE IV. – Major (wt%) and trace (ppm) elements geochemical data for the hybride zone at the Samapleu E1 zone. Data from CRPG Nancy, France

Drilling holes	SM24-661614						SM24 628688		SM24 645670	
Lithologies	Hybrid facies				Sapphirine hybride facies					
Samples	SM24 /309	SM24 /315.2	SM24 /281	SM24 /279.5	SM24 /291	SM24 /303.5	SM24(4) /33.4	SM24(4) /37	SM24(3) /30.7	SM24 (3) /48.7
Depth (m)	-309	-315.2	-281	-279.5	-291	-303.5	-33.4	-37	-30.7	-48.7
SiO_2	55.85	53.30	54.70	54.09	45.52	49.55	49.14	38.88	50.30	43.43
TiO_2	0.07	0.34	0.15	0.11	0.14	0.20	0.59	0.51	0.33	1.10
Al_2O_3	23.86	16.13	14.46	15.60	25.58	9.99	17.23	32.94	9.58	25.28
Fe_2O_3	3.01	10.17	10.17	9.87	8.05	13.70	13.53	8.88	14.29	8.76
MnO	0.05	0.13	0.17	0.14	0.12	0.19	0.18	0.10	0.25	0.09
MgO	3.30	11.71	13.97	12.62	12.28	21.43	14.44	13.96	22.31	14.15
CaO	8.31	4.79	4.19	4.59	5.11	2.03	4.12	3.10	1.92	4.39
Na_2O	4.95	3.25	2.71	3.09	2.31	0.78	1.73	1.85	0.59	1.68
K_2O	0.61	0.39	0.37	0.30	0.32	0.21	0.14	0.17	0.04	0.11
P_2O_5	ld	ld	ld	ld	ld	ld	ld	0.03	ld	ld
LOI	0.60	0.32	0.00	0.17	0.93	0.47	-0.49	0.20	-0.47	0.03
Ni	65.23	251.10	135.60	576.50	125.80	920.70	49.45	73.36	228.20	45.79
Co	14.18	46.53	29.98	42.83	27.96	53.43	42.09	25.55	53.68	27.24
Cr	45.14	649.90	190.60	367.60	64.36	515.10	61.28	60.16	173.20	65.45
Cu	214.90	526.00	56.25	714.30	62.90	643.40	22.78	9.87	27.33	29.70
Zn	41.42	127.50	113.80	109.70	144.60	163.70	153.00	111.10	183.00	100.10
Ba	408.20	339.30	219.60	304.00	225.10	571.50	112.90	166.60	45.59	158.90
Rb	3.12	2.68	4.17	3.29	3.74	8.34	1.54	1.24	0.56	1.49
Sr	528.40	394.00	284.90	414.60	266.80	137.10	197.40	189.20	96.66	420.30
Pb	8.47	6.58	4.67	3.89	6.20	32.54	2.55	3.13	0.93	2.53
Hf	0.38	1.23	1.83	2.39	4.58	1.68	1.77	4.80	2.93	17.55
Nb	0.40	4.52	1.14	0.93	0.21	1.23	5.67	13.09	5.33	27.88
Ta	0.04	0.32	0.14	0.10	0.03	0.23	0.48	1.29	0.41	2.39
Th	0.35	0.19	0.55	0.14	0.17	0.11	0.22	0.42	0.08	1.32
U	0.08	0.17	0.28	0.12	0.29	0.07	0.15	0.23	0.10	0.32
V	20.51	103.20	74.58	60.63	52.15	138.80	148.90	112.70	132.40	120.20
Y	1.67	4.00	3.66	2.06	3.44	2.55	4.53	2.92	3.68	2.08
Zr	15.02	46.27	70.76	94.69	186.30	64.82	63.29	199.00	118.60	752.70
La	26.55	21.09	13.30	8.96	18.18	6.89	9.39	15.86	3.17	15.63
Ce	38.58	30.82	20.69	12.10	27.94	9.28	14.81	23.90	5.01	20.45
Nd	11.05	9.28	6.33	3.25	8.71	2.79	4.48	7.09	1.64	5.29
Sm	1.27	1.19	0.89	0.43	1.11	0.38	0.66	0.83	0.32	0.62
Eu	1.43	1.07	0.73	0.72	0.77	0.26	0.50	0.70	0.18	0.90
Gd	0.68	0.87	0.67	0.32	0.74	0.34	0.63	0.55	0.37	0.40
Tb	0.08	0.12	0.10	0.05	0.10	0.05	0.10	0.08	0.07	0.06
Dy	0.36	0.70	0.58	0.31	0.57	0.37	0.69	0.45	0.52	0.33
Ho	0.06	0.14	0.12	0.07	0.12	0.09	0.15	0.09	0.13	0.07
Er	0.16	0.44	0.39	0.25	0.37	0.33	0.50	0.33	0.43	0.25
Tm	0.02	0.07	0.07	0.05	0.07	0.07	0.09	0.06	0.08	0.05
Yb	0.17	0.56	0.52	0.41	0.50	0.56	0.69	0.49	0.66	0.38
Lu	0.03	0.10	0.09	0.08	0.09	0.11	0.12	0.10	0.12	0.07

*Note: (1) ld = detected limit; (2); nd = not determined

K_2O and Na_2O continue to increase but remain very low (0.5 and 0.2% respectively). The third trend in gabbro-norites shows an increase of SiO_2, Al_2O_3, Na_2O, K_2O and TiO_2, and a decrease of CaO and FeO, again reflecting crystallization from more evolved liquids.

Mineralization

Fifty samples were collected from boreholes SM44-450250b, SM44-505224 (zone SM) and from boreholes SM24-661614, SM24-628651and SM25-009620 (zone E1).

Sulfide mineralization was first characterised visually from the core material and then microscopically on polished thin sections using reflected light microscope at the University of Franche-Comté in France. Sulfides and Platinoid group minerals (PGM) compositions were assessed by X-ray dispersion spectrometry (EDS) using scanning electron microscope (SEM) and electron microprobe of the Bureau de Recherche Géologique et Minière (BRGM) of Orléans, France.

Base metal sulfides

At the SM and E1 deposits, sulfides appear as disseminated in practically all rocks of the intrusion. They display a matrix texture and are interstitial to silicates and/or oxides when their abundance is less than 10% (fig. 8a). When modal proportions are 10-30%, especially in the pyroxenites, sulfide partially or totally encloses the surrounding silicates and/or oxides and displays a net texture (fig. 8b). Within the pyroxenite facies, sulfides also occur as semi-massive (30-60% sulfide) to massive (>60% sulfide) veinlets or lenses of centimetric to plurimetric sizes (fig. 8c). In such cases, lenses show irregular but sharp contacts with the surrounding rock, and brecciated textures are often observed near contacts. In these breccias, rounded and angular fragments of pyroxene or olivine are enclosed within a sulfide matrix (fig. 8d). Sulfide inclusions in olivine, pyroxene and/or oxides minerals and trails of sulfides nodules impregnating microfractures in silicates are also observed. Small sulfide veins (<4 mm in thickness) are frequently seen in silicate minerals as anastomosing networks. Finally, chalcopyrite-rich sulfide veins crosscut silicates and oxide minerals (fig. 8e).

Sulfide phases are, in order of abundance, pyrrhotite, pentlandite, chalcopyrite and a small amount of pyrite. Mackinawite and parkerite (substitution phases for pentlandite and pyrrhotite) are accessory minerals. *Pyrrhotite* is the most abundant mineral. It constitutes the main matrix for other sulfides and forms large poikilitic and xenomorphic crystals (fig. 8f). It also occurs as small rounded inclusions in silicate minerals. *Pentlandite*, the second mineral in abundance, appears essentially together with pyrrhotite but also in contact with chalcopyrite, pyrite and silicates (fig. 8f). It is present as xenomorphic crystals in irregular veinlets and as exsolutions along fractures within pyrrhotite grains. *Chalcopyrite* is the third mineral of global abundance but the main mineralised phase in late sulfide veins crosscutting silicates and chromites. Chalcopyrite is also present either as grains of 100 microns (μm), or as large xenomorphic phases and irregular veinlets in pyrrhotite (fig. 8f). *Pyrite,* when present, occurs as small automorphic to sub-automorphic (100-300 μm) crystals in pyrrhotite and at contacts with chalcopyrite or pentlandite. These grains are monocrystalline but display a polycrystalline habit in net-textured sulfide.

The sulfide grains are polyphase regardless of the mineralization type; disseminated, semi-massive or massive. Chalcopyrite veins correspond to the last stages of crystallisation of sulfides.

Ni and Cu grades vary from 0.2% to 0.6% for disseminated sulfide, 1 to 2% for semi-massive and massive sulfide lenses. Maximum values are 4,11% Ni and 6,18% Cu (tab. VI). Mineral resources established by Sama Nickel-CI in August 2013, representing only the near surface portions of the SM and E1 deposits, exceed 40 million tons grading 0.25% Ni and 0.22% Cu. Mineralization is open laterally at the E1 as well as extending at depth at both the SM and E1 deposits. Samapleu deposits are compared to other world-class deposits in table VI.

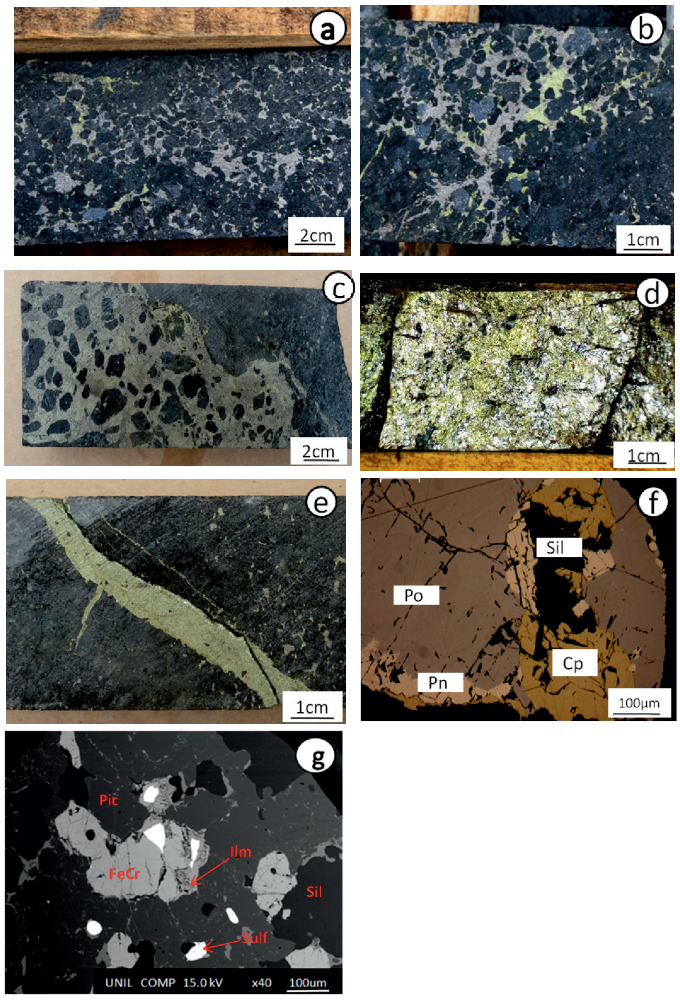

FIG. 8. – Photography of various sulfide textures and oxides observed at the Samapleu deposits. A: matrix texture; b: net texture; c: breccia texture; d: massive sulfide; e: late chalcopyrite veins; f: photomicrographs in reflected light of pyrrhotite (Po), pentlandite (Pn), chalcopyrite (Cp), Sil (silicates); g: chromitites (UNIL microprobe). Pic = picotite; FeCr = ferrochromite; Ilm = ilménite; Sulf = sulfure.

TABLE V. – Chemical results of the sulfide rich rock at the Samapleu sequence.

Lithologies	Drilling holes	From (m)	To (m)	Thickness (m)	Ni (%)	Cu (%)	Pd (ppb)	Pt (ppb)	Pt/Pd	Pd/Pt
Olivine pyroxenites	SM24-661614	71.5	72.25	0.75	0.2	0.08	740	160	0.22	4.62
		87	88.4	1.4	0.19	0.06	240	40	0.17	6
	SM24-628651	79.4	80.55	1.1	0.23	0.02	460	90	0.20	5.11
Chromite pyroxenites	SM24-661614	99.17	99.9	0.73	0.26	0.1	690	270	0.39	2.56
		103.5	104.3	0.8	0.24	0.28	440	170	0.39	2.59
		112	112.65	0.65	0.17	0.24	480	1420	2.96	0.34
Sulfide pyroxenites	SM24-661614	138	139	1	0.22	0.14	260	50	0.19	5.2
		144	145	1	0.36	0.65	490	50	0.10	9.8
		150	151	1	0.35	1.01	670	60	0.09	11.17
		159	160	1	0.15	0.09	110	40	0.36	2.75
	SM44-450250 (b)	60	61	1	0.795	0.365	490	160	0.33	3.06
		62	63	1	0.165	0.25	90	100	1.11	0.9
		65.4	66	0.6	0.455	0.445	570	70	0.12	8.14
		69	70	1	0.15	0.275	110	90	0.89	1.22
		73.05	74	0.95	0.24	0.38	400	90	0.23	4.44
Semi-massif sulfides	SM24-661614	162	163	1	1.49	0.71	2360	40	0.02	59
		168	169	1	1.71	1.17	2620	60	0.02	43.67
		170	170.6	0.6	1.33	0.85	1930	70	0.04	27.57
	SM24-628651	63.4	64	0.6	0.78	0.16	1430	280	0.20	5.107
		65	66.1	1.1	1.6	0.59	2460	1390	0.57	1.77
		90.5	90.75	0.3	2.22	0.14	2380	90	0.04	26.44
		90.95	91.25	0.3	2.35	0.19	2150	20	0.01	107.5
		104	104.5	0.5	0.39	0.3	400	70	0.12	5.71
	SM44-450250 (b)	45.1	45.4	0.3	3.37	0.78	1870	20	0.01	93.5
		91.25	91.9	0.65	2.16	1.51	1940	70	0.04	27.71
Massif sulfides	SM44-450250 (b)	76.9	77.3	0.4	4.11	1.54	2760	10	0.004	276
		85.25	86	0.75	4.04	6.18	3450	10	0.003	345
		86	87	1	3.92	5.29	3390	10	0.003	339
		87	87.9	0.9	4.4	2.84	2730	1530	0.56	1.78
		88.4	89	0.6	3.1	2.12	2710	90	0.033	30.11
		89.75	90.5	0.75	4.29	1.83	3610	20	0.006	180.5

Chromitites

Chromitites are also present as sub-parallel thin layers ranging from 1 to 50 cm in thickness with sharp and well-defined geological contacts with other ultramafic facies. The chromite content can exceed 70% and is often associated with ilmenite and magnetite (fig. 8g).

Platinum Group Minerals (PGM)

High tenors of platinum group elements (PGE), notably palladium and platinum were revealed during the chemical analysis of mineralised samples (tab. VI). These elements are found in platinum group minerals, which occur as small euhedral, rarely anhedral inclusions (10-20 μm) in sulfides, silicates, or at silicate-sulfide and chromite-sulfide interfaces.

The main platinum group minerals are Pd-Pt bismuthotellurides (michenerite, merenskyite, moncheite), Rh rich cobaltite-gersdorffite, irarsite and the hollingworthite (fig. 9, tab. VII). Minor species identified by Ouattara [1998] include mertieite, kotulskite, laurite, majakite, malanite and the soboleskite. Irarsite and hollingworthite are found as exsolution within the cobaltite-gersdorffite. Sperrylite was identified by SEM, associated with chromitite.

Most of the PGM are enriched in Pd and to a lesser extent in Pt and Rh. The palladium rich minerals are found in all sulfide types; disseminated, semi-massive and massive. Platinum rich minerals are rare and were observed exclusively in the chromite and sulfide-rich websterites. Michenerite, merenskyite and moncheite also contain minor amounts of Sb, Ni, Cu, Fe and S.

TABLE VI. – Samapleu deposits versus other world class deposits using Ni-Cu tenors and tonnages.

Deposits	Country	Status	Tonnages and Tenors
Jinchuan	China	Production	515 Million tons @ 1.06% Ni, 0.67% Cu
Voisey's Bay	Canada	Production	142 Million tons @ 1.59% Ni, 0.85% Cu
Mirabela	Brazil	Production	130 Million tons @ 0.60% Ni, 0.16% Cu
Tati	Botswana	Production	48 Million tons @ 0.59% Ni, 0.34% Cu
Mt Keith	Australia	Production	503 Million tons @ 0.55% Ni, 0.01% Cu
Talvivaara	Finland	Production	1.004 Million tons @ 0.22% Ni, 0.13% Cu
Noril'sk	Russia	Production	1.903 Million tons @ 1.77% Ni, 3.57% Cu
Aquablanca	Spain	Maintenance	8 Million tons @ 0.65% Ni, 0.50% Cu
Samapleu	Côte d'Ivoire	Exploration	40 Million tons @ 0.25% Ni, 0.22% Cu

U/Pb dating on zircon and rutile

One of the keys to understanding the geodynamic environment of the Samapleu intrusion is its age and its timing relative to the evolution of the Man craton. Previously the craton had been dated only imprecisely, at 3.5 to 2.7 Ga [Kouamelan *et al*., 1997; Pitra *et al*., 2010]. Ouattara [1998]

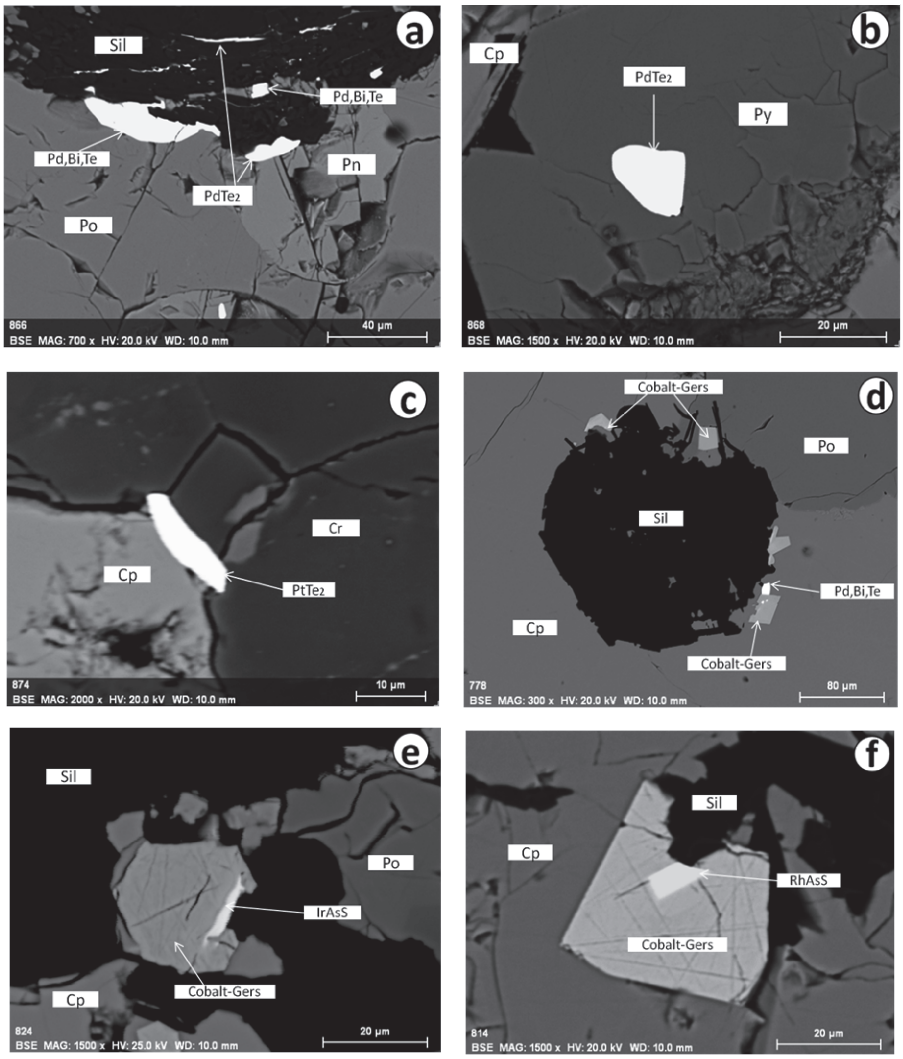

FIG. 9. – Microphotographs of various elements of the Platinum Group Minerals (PGM) at the Samapleu deposits obtained by scanning electron microscope. a: michenerite within Po on contact with silicate; merenskyite within Pn on contact with silicate and as dragged; b: merenskyite within pyrite; c: moncheite at the interface between chalcopyrite and chromite; d: (Rh, Pd) cobaltite-gersdorffite within (Cp, Po) sulfides; e: irarsite exsolution within cobaltite-gersdorffite; f: hollingworthite exsolution within cobaltite-gersdorffite. Sil = Silicate; Cr = chromite; Po = pyrrhotite; Pn = pentlandite; Cp = chalcopyrite; Cobalto-Gers = cobaltite-gersdorffite; RhAsS = hollingworthite; IrAsS = irarsite; PtTe2 = moncheite; PdTe = merenskyite; Pd,Bi,Te = michenerite.

noted a lack of metamorphism at the Samapleu intrusion and proposed that it was younger than the last major metamorphic event, the Liberian orogeny at 2.9-2.7 [Pitra *et al.*, 2010].

TABLE VII. – Main characteristics for the PGM assemblages, Samapleu deposit.

PGM mineralization types	Formulas	Number of grains	Host minerals				Host lithologies
			A	B	C	D	
Michenerite	$(Pd,Pt,Ni,Fe,Cu)_1(Bi,Sb)_1(Te,S)_1$	16	●	●			- Massive sulfides -Semi-massive sulfides -Sulfide websterites
Moncheite	$(Pt,Ni,Rh)_1(Te,Bi,Sb,Pb)_2$	6	●		●		- Sulfide chromitites
Rh-Cobaltite-gersdorthite	(Rh,Pd,Co,Ni,Fe)AsS	13	●	●			- Massive sulfides -Semi-massive sulfides
Irarsite	(Ir,Rh,Pd,Pt)AsS	1				●	- Massive sulfides
Hollingworthite	(Rh,Pt,Pd,Ir)AsS	1					- Massive sulfides
Merenskyite	$(Pd,Pt,Ni,Cu,Fe)_1(Te,Bi,Sb,S)_2$	12	●	●	●		- Massive sulfides -Semi-massive sulfides -Sulfide websterites -Sulfide chromitites

A = Inclusion in sulfides mineral
B = Interface between silicate-sulfides
C = Interface between silicate-chromites
D = intergrown with PGM

● Symbol size reflects the relative abundance of each

To obtain a better age for the intrusion, additional geochronology studies were undertaken at the Laboratoire Magmas et Volcans in Clermont-Ferrand, France (tab. VIII). Zircons and rutiles were extracted by crushing, sieving and the use of heavy liquids from samples SM24-278 (hybrid facies) and SM24-339 (granulite-gneiss) in borehole SM24-661614 (E1 sequence) near the contact between the mafic-ultramafic sequence and the gneiss (ref. fig. 4a). The collected zircon grains are euhedral or prismatic with sizes ranging between 50 and 200 µm (fig. 10a).

U-Th-Pb isotopic data for the zircons and rutiles were obtained by laser ablation inductively coupled plasma spectrometry (LA-ICPMS). The analyses involved the ablation of minerals with a Resonetics Resolution M-50 powered by an ultra-short-pulse (< 4ns) ATL Atlex Excimer laser system operating at a wavelength of 193 nm [detailed description in Müller et *al.*, 2009]. The ablated material was carried into helium and then mixed with nitrogen and argon before injection into the plasma source of an Agilent 7500 cs ICP-MS equipped with a dual pumping system to enhance sensitivity. Spot diameters of 26 µm and 44 µm associated to repetition rates of 3 Hz and fluency of 6 J/cm^2 were used for zircon and rutile dating respectively. Raw data was carried out with the software package GLITTER® from Macquarie Research Ltd [van Achterbergh *et al.*, 2001; Jackson *et al.*, 2004]. Calculated ratios were exported and Concordia ages and diagrams were generated using Isoplot/Ex v. 2.49 software package by Ludwig [2001].

TABLE VIII. – Zircon U-Pb data obtained by in situ laser ablation ICP-MS.

SM24-278 Zircon						**2 ? error**		**2 ? error**	**Age (Ma)**	**2? error**
sample	**Pb ppm**[1]	**Th ppm**[1]	**U ppm**[1]	**Th/U**	**^{207}Pb/^{235}U**[2]	**^{207}Pb/^{235}U**	**^{206}Pb/^{238}U**[2]	**^{206}Pb/^{238}U**	**^{207}Pb/^{206}Pb**	**^{207}Pb/^{206}Pb**
278/01 center	551	66	657	0.10	30.927	1.123	0.7206	0.0265	3527	46
278/02 center	1041	592	1122	0.53	31.608	1.146	0.7244	0.0266	3553	46
278/03 point	734	393	1333	0.29	16.149	0.587	0.4754	0.0175	3161	48
278/04 center	47	29	89	0.33	12.511	0.470	0.4719	0.0174	2761	52
278/05 center	92	83	150	0.56	13.617	0.508	0.5127	0.0189	2765	51
278/06 center	1362	532	1617	0.33	27.585	0.999	0.6982	0.0255	3399	47
278/07 rim	81	51	135	0.38	14.282	0.527	0.5265	0.0194	2799	50
278/08 center	107	84	169	0.50	14.578	0.534	0.5391	0.0198	2794	50
278/09 center	65	39	112	0.35	12.999	0.478	0.5148	0.0189	2681	51
278/10 center	752	374	1302	0.29	13.589	0.493	0.5197	0.0190	2739	50
278/11 center	784	572	1070	0.53	19.173	0.695	0.6051	0.0221	3051	48
278/12 center	87	58	139	0.42	14.838	0.548	0.5432	0.0199	2810	51
278/13 center	91	53	148	0.36	14.566	0.534	0.5385	0.0197	2794	50
278/14-1 rim	60	22	71	0.31	29.649	1.117	0.6873	0.0255	3535	49
278/14-2 center	29	13	34	0.38	27.895	1.077	0.6919	0.0259	3430	52
278/15 center	116	79	189	0.42	14.412	0.531	0.5318	0.0194	2798	51
278/16 center	81	90	126	0.71	13.719	0.507	0.5185	0.0190	2758	51
278/17 center	125	81	201	0.41	14.573	0.535	0.5404	0.0197	2789	50
278/18 center	36	24	62	0.39	13.444	0.506	0.5128	0.0188	2743	53
278/19 center	223	135	368	0.37	14.294	0.522	0.5316	0.0194	2785	50
278/20 center	188	115	309	0.37	14.304	0.523	0.5306	0.0193	2789	50
278/21 center	125	78	203	0.38	14.394	0.526	0.5332	0.0194	2791	50
278/22 center	262	161	385	0.42	19.301	0.709	0.5594	0.0204	3186	49
278/23 center	145	31	290	0.11	12.708	0.472	0.4696	0.0171	2795	52
278/24 center	477	245	675	0.36	20.340	0.743	0.5946	0.0216	3173	49
278/25 center	149	89	152	0.58	33.349	1.220	0.7424	0.0270	3597	47
278/26-1 center	601	388	623	0.62	32.141	1.170	0.7303	0.0265	3566	47
278/26-2 rim	151	67	242	0.28	18.134	0.674	0.5379	0.0196	3149	50
278/27 center	541	230	868	0.26	17.619	0.644	0.5438	0.0197	3086	49
278/28 center	36	19	59	0.32	14.586	0.548	0.5402	0.0197	2792	53
278/29 rim	495	79	737	0.11	21.565	0.788	0.5809	0.0210	3301	49
278/30 center	233	117	370	0.31	18.705	0.690	0.5297	0.0192	3223	50
278/31 center	256	178	254	0.70	33.958	1.241	0.7481	0.0271	3613	47
278/32 center	29	13	51	0.25	13.292	0.508	0.5120	0.0187	2727	54
278/33 center	129	59	153	0.39	27.934	1.025	0.6865	0.0248	3445	48
278/34 center	1208	106	1802	0.06	20.419	0.746	0.6147	0.0222	3126	49
278/35 center	336	241	378	0.64	27.725	1.016	0.6837	0.0247	3439	48
278/36 center	244	94	294	0.32	27.137	0.996	0.6815	0.0246	3411	49
278/37 center	80	54	132	0.41	14.170	0.527	0.5262	0.0190	2787	52
278/38 center	2556	838	2892	0.29	32.472	1.189	0.7226	0.0260	3598	48
278/39 center	905	85	1365	0.06	20.450	0.750	0.6068	0.0218	3149	50
278/40 center	617	139	1016	0.14	16.731	0.615	0.5497	0.0198	2986	51

[1]: concentration uncertainty c.20%
[2]: data not corrected for common-Pb
Decay constants of Jaffrey *et al.* [1971] used

TABLE VIII (suite). – Zircon U-Pb data obtained by in situ laser ablation ICP-MS.

SM24-339 Zircon						2 ? error		2 ? error	Age (Ma)	2 ? error
sample	Pb ppm[1]	Th ppm[1]	U ppm[1]	Th/U	$^{207}Pb/^{235}U$[2]	$^{207}Pb/^{235}U$	$^{206}Pb/^{238}U$[2]	$^{206}Pb/^{238}U$	$^{207}Pb/^{206}Pb$	$^{207}Pb/^{206}Pb$
339/01 center	92	193	114	1.70	14.467	0.536	0.5375	0.0191	2787	53
339/03 center	41	98	47	2.08	14.738	0.560	0.5450	0.0195	2794	55
339/04 center	80	177	96	1.84	14.589	0.543	0.5390	0.0192	2796	54
339/05 center	35	89	39	2.31	14.551	0.560	0.5371	0.0193	2797	56
339/06 center	143	334	173	1.93	14.157	0.527	0.5225	0.0186	2797	54
339/07 center	103	164	139	1.18	14.517	0.543	0.5408	0.0192	2782	54
339/08 center	59	149	63	2.38	14.821	0.560	0.5439	0.0194	2806	55
339/09 center	21	49	25	1.96	14.680	0.554	0.5418	0.0196	2797	55
339/10 rim	126	321	140	2.29	14.413	0.514	0.5403	0.0192	2772	50
339/11 center	82	171	101	1.69	14.692	0.527	0.5411	0.0193	2801	51
339/12 center	167	540	158	3.41	14.495	0.518	0.5361	0.0191	2794	50
339/13 center	264	482	345	1.40	14.397	0.510	0.5343	0.0189	2788	50
339/14 rim	28	48	36	1.32	14.688	0.547	0.5407	0.0194	2801	53
339/15 center	122	239	154	1.55	14.548	0.519	0.5355	0.0190	2802	50
339/16 center	27	64	30	2.11	14.279	0.554	0.5347	0.0194	2773	57
339/17 center	27	55	33	1.68	14.324	0.539	0.5338	0.0192	2782	54
339/18 center	106	178	142	1.25	14.377	0.515	0.5362	0.0191	2780	50
339/19 rim	82	206	103	2.01	13.271	0.492	0.5013	0.0180	2759	53
339/20 center	85	204	98	2.09	14.430	0.521	0.5352	0.0191	2789	51
339/21 center	56	143	61	2.36	14.678	0.533	0.5437	0.0194	2791	51
339/22 center	159	344	199	1.73	13.982	0.500	0.5270	0.0187	2763	50
339/23 center	123	247	157	1.57	14.384	0.518	0.5302	0.0189	2799	51
339/24 rim	232	385	317	1.22	14.389	0.516	0.5322	0.0189	2794	50
339/25 center	12	18	15	1.14	15.098	0.604	0.5500	0.0202	2819	59
339/26 center	104	189	135	1.40	14.570	0.526	0.5412	0.0193	2787	51
339/27 center	114	222	155	1.44	13.728	0.493	0.5088	0.0181	2790	51
339/28 center	79	220	82	2.69	14.556	0.531	0.5374	0.0192	2797	52
339/29 center	210	458	252	1.81	14.510	0.521	0.5394	0.0192	2785	51
339/30 center	33	84	36	2.31	14.382	0.545	0.5321	0.0192	2793	55
339/31 center	182	389	221	1.76	14.349	0.517	0.5387	0.0191	2769	51
339/32 center	98	206	120	1.71	14.422	0.525	0.5343	0.0191	2791	52
339/33 center	21	49	26	1.91	13.493	0.543	0.5075	0.0186	2766	59
339/34 center	111	223	138	1.62	14.563	0.530	0.5399	0.0192	2790	52
339/35 center	75	213	76	2.81	14.412	0.528	0.5376	0.0192	2780	52
339/36 center	155	427	159	2.68	14.454	0.527	0.5400	0.0192	2777	52
339/38 center	334	754	456	1.65	13.212	0.483	0.4893	0.0174	2792	52
339/39 center	70	186	94	1.98	12.222	0.491	0.4668	0.0171	2741	59

[1]: concentration uncertainty c.20%
[2]: data not corrected for common-Pb
Decay constants of Jaffrey *et al*. [1971] used

Zircons from the gneiss yielded an age of 2784 ± 7 Ma, similar to the age published by Kouamelan *et al*. [1997]; Pitra *et al.* [2010] (fig. 10b). Zircons from the hybrid facies gave ages ranging from 2.78 to 3.6 Ga. Rutile from the gneiss gave a $^{207}Pb/^{206}Pb$ age of 2091 ± 18 Ma identical to that of rutile from the hybrid zone 2090 ± 25 Ma (fig. 10b). Some individual and discordant rutile ages are older, but they are systematically lower than the 2.78 Ga measured in most zircons.

DISCUSSION

The Samapleu mafic to ultramafic sequence were intruded within the Archean gneiss and granulitic assemblage, which implies that the Samapleu sequence is younger than 2.78 Ga. The intrusion consists of peridotites, pyroxenites and gabbro-norites with cumulus textures.

In the E1 site, it extends for more than 2 km at the surface and varies from 50 m to 200 m in thickness (fig. 3a, b – 4a, b). It dips at 70°-80° and has been traced to a depth of at least 500 m. The mineralization, mainly pyrrhotite, pentlandite, chalcopyrite with a small amount of pyrite, PGM and some chromite, are mainly associated with pyroxenites. The sulfides display matrix or net-textures, or occur as droplets or in breccia. This suggests that the sulfide mineralization is magmatic and formed by immiscibility due to the production of early sulfide liquid from mafic and ultramafic silicate melts, as described by Naldrett [1989]. Upon formation and accumulation, the sulfide liquid migrated through the silicate sequence and impregnated the already crystallised olivine-pyroxene-chromite rich hosts. This information, together with the sub-vertical upward-anastomosing layout of mineralised veins and lenses, and the mineralization alignment with the regional fabric, suggest that sulfide melt migrated through a sub-vertical drainage system in the already crystallized silicate sequence.

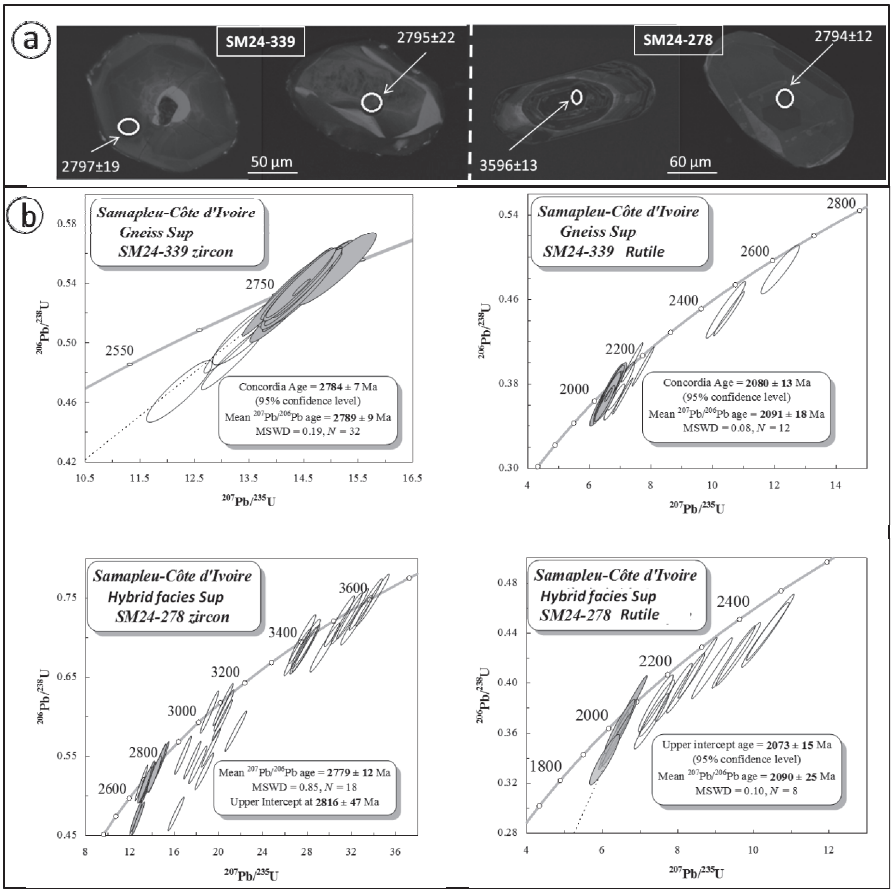

FIG. 10. – Radiochronologic analysis performed in the LMV in Clermont Ferrand University on gneisses and the hybride zone of the E1 zone at the contact between the intrusion and the surrounding rocks. A– Pictures of selected zircon grains; the circles represent the position of laser spots used for age determination, and the associated values are the resulting $^{207}Pb/^{206}Pb$ age (in Ma). B – Concordia plots ($^{206}Pb/^{238}U$ vs. $^{207}Pb/^{235}U$) performed from zircons and rutile.

The presence of sapphirine-cordierite-spinel and sillimanite within the hybrid zone is indicative of a metamorphic recrystallization of the gneissic protolith under medium pressure and high temperature (around 7-8 kbar and 700 to 950ºC; Gouedji [2014]). This is indicative of a meta-sediment origin for the alumina rich gneissic host (fig. 6) and could therefore explain the presence of multiple generations of inherited zircon with ages from 3.6 to 2.78 Ga. These observations suggest that crystallization of the Samapleu intrusion took place in the lower continental crust at a depth of approximately 25 km under P-T conditions typical of either the upper amphibolite to granulitic metamorphic conditions. This hypothesis could also explain "granoblastic" textures, triple-joint contacts between minerals and the undulating extinctions observed in pyroxenes and olivine of the Samapleu sequence.

Concerning the magmatic story, the major-element distribution in ultramafic to mafic rocks shows differentiation trends dominated by early olivine crystallization followed by pyroxene crystallisation with lesser amount of olivine or plagioclase, and final crystallisation of clinopyroxene, orthopyroxene and plagioclase (fig. 7). These trends suggest that the lherzolites and pyroxenites have most likely resulted from a single and progressively evolved primitive magma. The gabbro-norite sequence could have evolved from the same magma but it is also possible that it formed following a second, more evolved magma injection. However, in the absence of chilled margins, it is difficult to estimate the composition of the parental magmas.

One approach proposed by Chai and Naldrett [1992] is to use the olivine compositions to estimate the MgO/FeO molar proportions for the magmatic liquid. The Mg-Fe distribution coefficient, $KD = (FeO/MgO)^{Ol} / (FeO/MgO)^{L} = 0.3 \pm 0.03$ is relatively insensitive to temperature, pressure, and liquid composition [Roeder and Emslie, 1970]. In the E1 olivine rich units, olivine compositions vary from Fo_{81} to Fo_{83} (tab. IX). Using the highest Mg# of olivine 0.83, the estimated Mg# of the equilibrium liquid is calculated to be 0.61. The intercept of the MgO vs FeO regression line suggests that the parental magma contained about 10 wt% MgO and 11 wt% FeO (fig. 11). Based on this MgO estimate and the lherzolite to websterite regression lines, the magma is estimated to contain 53 wt% SiO_2 and 0.65% TiO_2 (fig. 7).

To establish the composition for trace elements in parental magmas, Chai and Naldrett [1992] proposed to use TiO_2, which was estimated from the MgO calculation. However, tenors for the HFS elements in the Samapleu sequence are extremely low and show a distribution that is too erratic for a meaningful use. Bédard [1994] proposed another

method to estimate trace element contents of the equilibrium liquids with cumulates.This method considers global partition coefficients for trace elements between minerals and equilibrium liquids, the composition of trace elements in cumulates, modal proportions minerals (ø), the fraction of liquid trapped (TM) and a set of partition coefficients (D). It also assumes that there is a balance between the trace elements and the trapped liquid crystallized as a closed system. The liquid composition is determined by the formula $\mathbf{C_j^{liq} = C_j^{min/min/liq} D_j}$ with C_j^{liq} = concentration of element (j) in the liquid with a mineral cumulat, C_j^{min} = concentration of the element (j) in the mineral, and $^{min/liq}D_j$ = partition coefficient of the element (j) between the liquid and the mineral. The estimate of the modal proportion minerals is made by counting under a microscope. Hence, in Samapleu Extension 1 rocks, the fraction of trapped melt (TM) was considered 5% after comparing different calculated values for the trapped liquid lherzolites. The results suggest that primitive magma in equilibrium with lherzolites and olivine websterites had Ni contents from 148 to 417 ppm and Cr contents from 174 to 837 ppm (tab. X-XI). These are consistent with Ni and Cr contents of high MgO magmatic liquids, as determined by Chai and Naldrett's approach.

Hence, the estimated SiO_2, MgO, Cr and Ni contents suggest that the Samapleu parental magma was basaltic with around 10% of MgO. TiO_2 contents seem unusually low (TiO_2 = 0,65%; tab. X) but this is due to the fact that most of the rocks are cumulates. However, it could be also a mark of a low Ti parental magma as is known in subduction environments. Chondrite-normalized REE patterns and the MORB normalized spiderdiagrams using Bédard's [1994] partition coefficients returned strong LREE enrichment, flat HREE spectra, Ba, Rb, Th enrichments, and depletion of Ta-Nb (fig. 12). Such geochemical characteristics could mark a subduction environment but also and more probably a mantle plume origin followed by granite or sediment assimilation during emplacement in the continental crust [Thomson *et al.*, 1983; Hofmann, 1988; Voshage *et al.*, 1990; Arndt *et al.*, 1993; Borisova *et al.*, 2001; Li *et al.*, 2005; Lehmann *et al.*, 2007], which is consistent with the evidence of assimilation of gneiss in the hybrid zone. In accordance with Naldrett [1989, 2004], Song *et al.* [2011] and

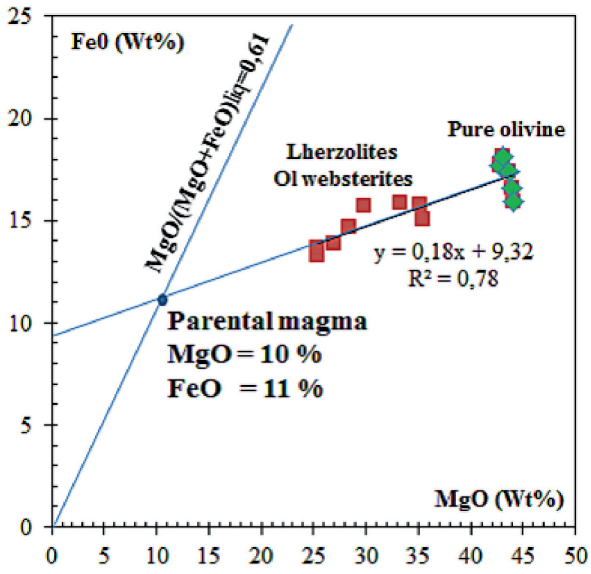

FIG. 11. – FeO and MgO diagram [Chai and Naldrett, 1992] extrapolating composition of the Samapleu sequence primary magma. The primary magma has a MgO content of ~9 wt% and FeO ~11 wt %.

TABLE IX. – Olivine chemical composition at the Samapleu E1 zone.

Rocks	Olivine websterite			Lherzolite	
Samples	SM1-67.8	SM24 -1-118.4	SM1-217.5	SM24 -1-83	SM1-182
SiO_2	39.23	39.30	38.33	39.66	38.44
TiO_2	0.01	0.02	0.02	0.02	0.01
Al_2O_3	0.00	0.02	0.01	0.05	0.00
Cr_2O_3	0.01	0.01	0.02	0.01	0.01
FeO	16.64	17.73	18.09	15.99	17.34
MnO	0.37	0.21	0.22	0.25	0.30
MgO	44.17	42.85	42.89	44.26	43.54
CaO	0.02	0.02	0.01	0.01	0.01
Na2O	0.01	0.07	0.02	0.05	0.02
K2O	0.01	0.03	0.01	0.03	0.01
NiO	0.15	nd	0.24	nd	0.30
Total	100.63	100.25	99.86	100.33	100.00
Si	0.99	1.00	0.98	1.00	0.98
Ti	0.00	0.00	0.00	0.00	0.00
Al	0.00	0.00	0.00	0.00	0.00
Cr	0.00	0.00	0.00	0.00	0.00
Fe	0.35	0.38	0.39	0.34	0.37
Mn	0.01	0.00	0.00	0.01	0.01
Mg	1.66	1.62	1.64	1.66	1.66
Ca	0.00	0.00	0.00	0.00	0.00
Na	0.00	0.00	0.00	0.00	0.00
K	0.00	0.00	0.00	0.00	0.00
Ni	0.00	nd	0.00	nd	0.01
Total	3.01	3.00	3.02	3.00	3.02
Fo	82.54	81.14	80.85	83.14	81.73
#Mg	0.83	0.81	0.81	0.83	0.82
Mg# of liquid	0.60	0.58	0.57	0.61	0.58

Fo = Forsterite content; Mg# of liquid = mole ratio of MgO/(MgO + FeO); nd = not determined

TABLE X. – Estimated chemical composition of the Samapleu and Jinchuan intrusion primary magmas.

Major elements (wt%)	SiO_2	TiO_2	Al_2O_3	$FeO+Fe_2O_3$	MgO	CaO	Na_2O	K_2O
Samapleu magma	53.0	0.65	16.0	11.0	10	13.5	0.6	0.2
Jinchuan magma*	50.8	1.00	12.5	12.2	11.5	10.3	1.3	0.8
Trace elements (ppm)	Sr	Rb	Zr	Y	Nb	Th	Cr	Ni
Samapleu magma	20 - 212	0-27	17-89	6 - 18	2.1 - 7.4	0.5 - 10	174 -837	148 - 417
Jinchuan magma*	200	30	100	20	8	01.4		400

*Jinchuan magma after that 5% of olivine (Fo_{84}) has crystallized [Chai and Naldrett, 1992].

TABLE XI. – Estimated chemical composition of the magmatic liquids in equilibrium together with mafic and ultramafic cumulates from E1 zone (SM24-661614 drill-core) in Samapleu using Bedard [1994] method.

Drilling holes	SM24-661614										
Lithologies	Lherzolite			Olivine Webstérite							
Samples	SM24 /83	SM24 /173,8	SM24 /182	SM24 /208.5	SM24 /108.2	SM24 /239	SM24 /76.7	SM24 /67.8	SM24 /118.4	SM24 /197.6	SM24 /217.5
Depths (m)	83	173,8	182	208.5	108.2	239	76.7	67.8	118.4	197.6	217.5
La	1.2	8.5	19.1	4.7	6.8	7.5	17.7	17.9	14.7	13.5	9.3
Ce	5.4	14.5	25.6	8.5	11.2	15.5	33.1	25.3	27.7	29.2	17.1
Nd	7.2	7.1	9.6	3.8	6.2	7.1	17.5	10.2	13.2	13.7	7.4
Sm	2.0	1.5	1.9	0.8	1.5	1.5	3.8	1.9	2.6	2.9	1.5
Eu	0.5	0.4	0.6	0.2	0.2	0.6	0.8	0.5	0.5	0.9	0.3
Gd	2.4	1.5	1.9	0.9	1.6	1.6	3.6	1.8	2.6	2.8	1.5
Tb	0.4	0.2	0.4	0.2	0.3	0.3	0.6	0.3	0.5	0.5	0.3
Dy	2.8	1.7	2.0	1.0	1.8	1.6	3.0	1.9	2.6	2.8	1.7
Ho	0.60	0.39	0.51	0.24	0.37	0.36	0.64	0.41	0.58	0.61	0.38
Er	1.8	1.1	1.4	0.8	1.2	1.1	1.8	1.3	1.6	1.8	1.1
Tm	0.3	0.2	0.2	0.1	0.1	0.2	0.2	0.2	0.2	0.3	0.2
Yb	1.9	1.2	1.6	0.8	1.0	1.2	1.5	1.4	1.6	1.9	1.2
Lu	0.3	0.2	0.3	0.1	0.2	0.2	0.2	0.2	0.2	0.3	0.2
Ba	25.5	49.7	119	132	95.7	108	57.1	32.4	14.9	54.6	28.9
Sr	37.8	58.9	122	20.5	83.9	45.9	212	108	90.3	65.3	48.3
V	30.7	18.6	32.1	32.4	37.4	19.3	26.1	18.2	16.7	22.0	20.9
Cr	663	577	809	729	837	258	370	346	174	302	204
Ti	5834	2602	3994	2289	3225	3984	3893	3109	2486	3139	2332
Ni	205	174	148	290	283	343	411	192	296	194	417
Co	58.9	51.5	52.8	69.9	72.5	77.4	53.1	56.5	89.4	56.4	65.7
Zr	17.0	46.3	65.8	23.2	34.8	26.6	59.2	89.3	51.1	51.8	33.8
Hf	0.90	1.19	1.11	0.55	0.82	0.65	1.31	1.80	1.00	1.13	0.69
Nb	-	-	2.9	2.1	-	5.6	4.1	7.4	3.7	5.2	6.3
Ta	ld	ld	0.6	0.1	ld	0.6	1.5	0.8	0.3	0.8	0.5
Th	ld	ld	5.0	ld	ld	ld	0.8	9.8	1.4	0.7	0.5
U	ld	ld	1.2	ld	ld	ld	ld	2.7	Ld	ld	ld
Y	15.6	11.7	16.7	6.4	10.3	10.4	17.7	11.8	15.5	17.1	10.6
Cs	ld	ld	ld	ld	ld	ld	ld	ld	Ld	ld	ld
Rb	0.0	11.6	26.6	18.8	0.0	15.6	5.0	6.3	0.0	9.3	13.9

Drilling holes	SM24-661614											
Lithologies	Webstérite						Chromite websterite	Plagioclase websterite			Gabbronorite	
Samples	SM24 /139	SM24 /156.5	SM24 /67.4	SM24 /97.8	SM24 /186	SM24 /274.8	SM24 /271	SM24 / 257.4	SM24 / 260.3	SM24 /266.3	SM24 /251	SM24 / 254.5
Depths (m)	139	156.5	67.4	97.8	186	274.8	271	257.4	260.3	266.3	251	254.5
La	2.6	6.6	12.6	10.6	12.3	19.5	45.0	10.1	23.7	27.8	10.7	11.7
Ce	6.4	15.8	21.9	16.3	19.4	24.1	63.3	14.7	53.1	38.8	19.2	17.8
Nd	4.0	7.4	8.7	7.3	8.8	8.0	19.4	5.1	19.2	14.2	11.2	9.0
Sm	0.9	1.4	1.6	1.4	1.8	1.5	3.3	0.9	2.9	2.4	2.6	2.3
Eu	0.3	0.7	0.4	0.3	0.3	0.3	3.1	0.3	0.6	0.5	1.0	0.7
Gd	0.9	1.5	1.4	1.4	1.5	1.4	3.3	1.0	2.5	2.1	3.1	2.9
Tb	0.2	0.3	0.2	0.3	0.3	0.3	0.5	0.2	0.5	0.4	0.6	0.5
Dy	1.1	1.7	1.4	1.6	1.6	1.7	3.1	1.2	2.4	2.0	3.6	3.5
Ho	0.2	0.4	0.3	0.4	0.3	0.4	0.6	0.3	0.5	0.4	0.8	0.8
Er	0.8	1.3	0.9	1.1	1.2	1.3	2.0	1.0	1.6	1.4	2.4	2.4
Tm	0.1	0.2	0.1	0.1	0.2	0.2	0.3	0.2	0.2	0.2	0.4	0.3
Yb	0.9	1.3	1.0	1.1	1.2	1.4	1.8	1.5	1.5	1.5	2.4	2.3
Lu	0.1	0.2	0.1	0.2	0.2	0.2	0.3	0.2	0.2	0.2	0.4	0.4
Ba	139	37.5	39.8	42.1	52.2	7649	1703	227	6831	922	358	1019
Sr	37.4	103	45.7	34.0	53.8	121.6	91.1	99.6	47.0	53.5	383	398
V	37.3	34.5	26.0	14.8	34.7	41.6	14.3	108.2	84.9	76.1	95.7	101.9
Cr	762.4	528	2319	35.9	772	626	294	2836	3947	1831	641	807
Ti	1936	2517	1988	2949	2916	3381	6557	2340	3692	3300	5246	5608
Ni	831	362	456	150	356	361	188	1112	416	429	171	207
Co	64.1	39.6	87.2	61.9	66.0	58.0	57.9	131.9	67.5	57.6	49.5	62.2
Zr	17.0	30.4	27.2	47.1	57.6	42.9	97.1	22.6	61.9	90.6	29.5	19.3
Hf	0.47	0.73	0.61	1.15	1.22	0.82	1.85	0.66	1.36	1.96	1.01	0.78
Nb	1.3	3.6	5.4	4.3	3.7	12.0	10.1	ld	7.1	6.1	5.2	5.4
Ta	0.1	0.2	0.7	0.3	0.3	1.7	0.9	0.2	0.6	0.8	0.2	0.2
Th	ld	ld	6.2	2.2	5.6	1.4	11.5	0.7	3.5	2.9	ld	ld
U	ld	ld	1.34	0.45	1.65	ld	3.47	ld	0.97	0.88	ld	ld
Y	7.1	10.8	8.9	9.7	10.6	11.5	17.9	8.6	14.6	12.9	22.3	21.0
Cs	ld	ld	ld	ld	ld	10.16	ld	ld	165.6	2.89	ld	ld
Rb	14.1	6.1	6.2	5.8	16.9	98.6	75.8	9.6	1125	34.1	38.8	12.6

*Note : ld = detection limit

many other authors, magma contamination with granulitic wall rocks could also have a link with the appearance of a sulfide rich liquid.

LILE enrichments and the presence of green pargasite and tschermackite within the Samapleu intrusion units are also consistent with fluid-rock interactions, which probably occurred during slow cooling of the magma in the deep crust. Relatively high Pd/Pt ratio in PGM also supports the assumption of an important role played by hydrothermal fluids during the mineralization process.

All these data, and the relative continuity of ultramafic to mafic sequences in Samapleu Main and Samapleu Extension 1 deposits and at the Yorodougou occurrence are in accordance that Samapleu intrusions could represent a feeder dyke, and not a sill as originally proposed by Ouattara [1998]. They are in accordance that the Samapleu sequence emplaced in the lower part of an Archean continental crust at a depth of around 25 km. Therefore, the Samapleu sequence appears as a possible feeder zone for the Yacouba layered complex.

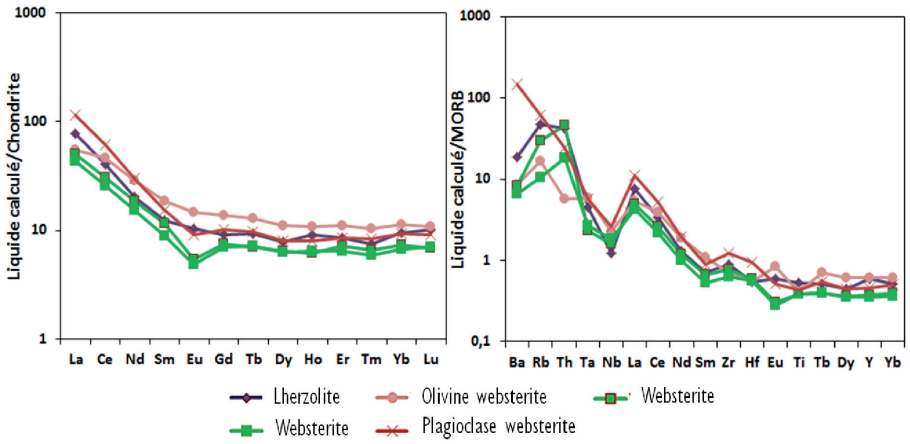

FIG. 12. – Rare earth and trace elements signatures of E1 lithological units at equilibrium [Bédard, 1994].

The U-Pb ages of 3.6 to 2.78 Ga obtained on zircons collected within the hybrid zone and in the gneiss assemblage, indicate an Archean history for the gneiss and for the protolith of the hybrid zone, with a last metamorphic event linked to the Liberian orogenesis (2.78 Ga). These ages are compatible with published age of 3.5 to 2.7 Ga for the Man Archean craton [Kouamelan, 1996; Kouamelan *et al*., 1997; Pitra *et al*., 2010]. Some individual and discordant oldest ages obtained on rutile and lower than the 2.78 Ga (measured in most zircons) can show both an inherited memory of the event at 2.78 Ga (metamorphic event) in the rutile, no reflect geological significance and only reflect the presence of a small common lead (Pb) component which could diverts a portion analytical point towards the Pb isotopic composition.

Moreover, the U-Pb age of 2.09 Ga obtained on rutile suggests that a younger metamorphic event took place. This is interpreted as the contact metamorphism between the Samapleu feeder dyke sequence and the gneissic host. This Eburnean age could then be the age of the intrusion for the Samapleu sequence and also the age of the metamorphic recrystallization observed within the hybrid zone. It also implies that ductile deformation affecting the area is either Eburnean or younger. This coincides well with the Eburnean ductile deformation observed south of the Man-Danané fault [Pitra *et al*., 2010]. Hence, the Samapleu intrusion could be linked to the Eburnean event observed south of the Man-Danané fault as first described by Pitra *et al*. [2010]. One hypothesis is that Samapleu magmas intruded Archean continental crust at 2.09 Ga during Birimian time¸ at the same period when an immense amount of mafic magma erupted throughout West Africa [Thiéblemont *et al*., 2004; Lompo, 2009-2010; Pitra *et al*., 2010]. These geodynamic events may then be related either to emplacement of the plume-related oceanic flood basalts of the Birimian sequence [Abouchami et *al*., 1990] or to the Eburnean tectonic convergence between the Birimian crust (currently central and eastern Côte d'Ivoire) and the Archean craton (currently western Côte d'Ivoire) between 2.1 and 2.05 Ga [Lompo, 2009-2010; Pitra *et al*., 2010].

Finally, emplacement of the Samapleu intrusion, the magmatic signature of the parental magmas, Ni-Cu sulfides properties and even PGM compositions, show strong similarities with Jinchuan deposit in China [Chai and Naldrett, 1992; Shibo and Halls, 1993; Li *et al*, 2005; Yang *et al,* 2006; Lehmann *et al.,* 2007]. The high Rh tenors (up to 9%) in the Samapleu cobaltites are comparable to those recorded in the Lukkulaisvaara layered complex in Russia (Rh up to 9 wt.%) [Barkov *et al.,* 1996], Pechenga (Rh close to 10.5 wt.%) [Distler and Laputina, 1979] and Pipe (*Manitoba*, Canada; Rh > 7.2 wt.%) [Cabri and Laflamme, 1981; Cabri, 1992].

CONCLUSION

The Samapleu mafic to ultramafic sequence, host of Ni-Cu-PGE mineralization, is composed of ultramafic to mafic sequences, ranging from peridotite units, pyroxene cumulates (websterite) and to plagioclase cumulates (norite and gabbro-norite).

Several Ni-Cu-PGE mineralized occurrences have been identified including the Samapleu Main deposit (SM), the Sama Nickel-CI discovered Samapleu Extension 1 (E1) deposit and the Yorodougou occurrence (Yo). Ni and Cu mineralization (pentlandite, chalcopyrite, combined with pyrrhotite, rarely pyrite) correspond primarily to sulfide disseminations mostly ranging from trace to 40% in pyroxenite facies. Semi-massive (40 to 80% sulfides) and massive sulfide rich lenses are, at least locally, spatially associated with highly breccia texture in pyroxenites. Sulfide mineralization display matrix, net-textures, droplets and breccia textures. They are characteristic of magmatic mineralization styles formed by immiscibility due to the production of early sulfide liquid from mafic and ultramafic silicate melts. Their textural relationships with silicates phases are indicative of "tardimagmatic" crystallization from immiscible sulfide liquid. Ni and Cu tenors vary from 0.2 to 0.6% for the disseminated sulfide; 1.0 to 2.0% for semi-massive to massive sulfide lenses, and can reach as much a 4.0% Ni and 4.0% Cu. Mineral resources established by Sama Nickel-CI in August 2013 exceed 40 million tons grading 0.25% Ni and 0.22% Cu representing only the near surface portions of the SM and E1 deposits.

PGM associated with the sulfide phases are either distinct mineral phases or as inclusions within sulfide species. PGM include Pt-Pd-tellurobismuthides, Pd-bismuthides,

Pd-arsenide-antimonides, Pd-arsenides, Rh-Pd-cobaltite-gersdorffite, Pt-telluride and other PGE-sulfides.

The concentric zonation (mafic in the center and ultramafic on the edge-zones E1), the habitus of the sulphured mineralization and the petro-chemical observations indicate that the Samapleu intrusion was emplaced as a feeder dyke.

The E1 hanging wall hybrid zone between ultramafic rocks and gneiss hosts, which is characterized by the presence of sapphirine and cordierite with trace of sillimanite, hercynite, rutile and/or ilmenite. It indicates that the Samapleu sequence was emplaced at a depth of about 20-25 km under granulitic metamorphic and crystallization.

The recalculated liquid compositions in equilibrium with ultramafic and mafic cumulates suggest moderate MgO basaltic parental liquids. The magmatic signature (major and trace elements) resembles a mantle plume magma that has assimilated abundant continental crust.

These mafic and ultramafic hosts were intruded at 2.09 Ga (U-Pb age on rutile), during Birimian time, within the older gneissic assemblage of the Man Archean terranes (U-Pb age of 2.78 Ga on zircon), at the same period when an immense amount of mafic magma erupted throughout West Africa. These geodynamic events may then be related either to emplacement of the plume-related oceanic flood basalts of the Birimian sequence [Abouchami *et al*., 1990] or to the Eburnean tectonic convergence between the Birimian crust (currently central and eastern Côte d'Ivoire) and the Archean craton (currently western Côte d'Ivoire) between 2.1 and 2.05 Ga [Lompo, 2009-2010; Pitra *et al*., 2010].

Samapleu Ni-Cu-PGE deposits present strong similarities with the Jinchuan complex in China (parental magma composition, complex form, sulfide and PGM mineralization type) [Chai and Naldrett, 1992; Shibo and Halls, 1993; Li *et al*., 2005; Yang *et al.,* 2006; Lehmann *et al.,* 2007…]. They could be also compared with Voisey's bay in Canada [Lambert et *al.,* 1999]; Kabanga deposit in Tanzania [Maier *et al*., 2010]; Nebo-Babel in Australia [Godel *et al*., 2011]; and the Nova deposit in granulite facies rocks of the Fraser range in Australia.

Exploration is presently ongoing in the area covered by the Sama Nickel-CI exploration permit. The newly discovered Yepleu, Gossan and Santa mineralized zones are mapping, drill holes are in progress, and the stratiform sequences of the Yacouba complex are working [Sama Nickel-CI; Picard, Gouedji, in progress – http://www.samaresources.com/s/Samapleu.asp].

Acknowledgements. – Our acknowledgements goes to Sama Resources Inc. which financed this research and particularly to its President and CEO, Dr. Marc-Antoine Audet, their Exploration Manager, M. Bakayoko Bouake and to the entire team of geologists and the support staff, without whom it would have been impossible to complete this study. We would like to mention the great help that we received from all the team at the laboratory Chrono-Environnement and especially Julien Baptist, a Master student, who participated actively in the research. We thank Nick Arndt and Kathleen Bartels for their valuable contributions to the English translation and revision of the manuscript. Many thanks to my supervisors and mentors; Professor Christian Picard from the UFR-STRM and Dr. Coulibaly of the FHB University in Abidjan. A world of thanks goes to Mr Alain Kouamelan, M. Djroh Cherubin and M. Allialy Marc Ephraim for the contributions to the research.

SGF associated editor: Romain Augier

References

Abouchami W., Boher M., Michard A. & Albarede F. (1990). – A major 2.1 Ga event of mafic magmatism in West Africa: An early stage of crustal accretion. – *J. Geophys. Res.,* **95**, 17605-17629.

Arndt N.T., Czamanske G.K., Wooden J.L. & Fedorenkof V.A. (1993). – Mantle and crustal contributions to continental flood volcanism. – *Tectonophysics,* **223**, 39-52.

Arndt N. & Ganino C. (2010). – Ressources minérales: Nature, origine et exploitation. – Dunod, Paris, 173 p.

Barkov A.Y., Men'shikov Yu. P., Begizov V.D. & Lednev A.I. (1996). – Oulankaite, a new platinum-group mineral from the Lukkulaisvaara layered intrusion, northern Karelia, Russia. – *Eur. J. Min.*, **8,** 311-316.

Bédard J.H. (1994). – A procedure for calculating the equilibrium distribution of trace elements among the minerals of cumulate rocks, and the concentration of trace elements in the coexisting liquids. – *Chem. Geol.,* **118**, 143-152.

Berger J., Diot H., Khalidou L., Ohnenstetter D., Féménias O., Pivin M., Daniel D., Bernard A. & Charlier B. (2013). – Petrogenesis of Archean PGM-bearing chromitites and associated ultramafic-mafic-anorthositic rocks from the Guelb el Azib layered complex (West African craton, Mauritania). – *Precamb. Res.,* **224,** 612-628.

Borisova A. Yu., Belyatsky B.V., Portnyagin M.V. & Sushchevskaya N.M. (2001). – Petrogenesis of olivine-phyric basalts from the Aphanasey Nikitin rise: Evidence for contamination by cratonic lower continental crust. – *J. Petrol.,* **42** (**2**), 277-319.

Cabri L.J. & Laflamme J.H.G. (1981). – Analyses of minerals containing platinum group elements, Chapter 8. *In*: L.J. Cabri, Ed., Platinum-group elements: Mineralogy, geology, recovery. – *Can. Inst. Mining and Metallurgy*, Sp. Vol. **23**, 151-173.

Cabri L.J. (1992). – The distribution of trace precious metals in minerals and mineral products. – The 23rd Hallimond Lecture (1991). – *Mineral. Mag.*, **56,** 298-308.

Camil J. (1984). – Pétrographie, chronologie des ensembles granulitiques archéens et formations associées de la région de Man (Côte d'Ivoire). – Thèse de doctorat, Université d'Abidjan, 306 p.

Carignan J., Hild P., Mevelle G., Morel J. & Yeghicheyan D. (2001). – Routine analyses of trace elements in geological samples using flow injection and low pressure on-line liquid chromatography coupled to ICP-MS: a study of geochemical reference materials BR, DR-N, UB-N, AN-G and GH. – *Geostand. Newslett.,* **25**, (2-3), 187-198.

Chai G. & Naldrett A.J. (1992). – The Jinchuan ultramafic intrusion: Cumulate of a high-Mg basaltic magma. – *J. Petrol.*, **33**, 277-303.

Coulibaly Y., Kouaho B., Gnanzou A., Allialy M.E. & Djro S.C. (2012). – Contexte géologique de la minéralisation aurifère du prospect de Bobosso (région de Dabakala, centre-nord de la Côte d'Ivoire). – *J. Rech. Sci*., Univ. Lomé (Togo), Serie A, **14** (2), 149-162.

Distler V.V. & Laputina I.L. (1979). – Nickel and cobalt sulpharsenides containing platinum metals. – *Dokl. Acad. Nauk*, ESS 24B, **3**, 718-721.

Godel B., Seat Z., Maier W.D. & Barnes S.-J. (2011). – The Nebo-Babel Ni-Cu-PGE sulfide deposit (West Musgrave block, Australia): Pt. 2. Constraints on parental magma and processes, with implications for mineral exploration. – *Econ. Geol.,* **106**, 557-584.

GOUEDJI G.E.F. (2014). – Les séquences mafiques-ultramafiques de Samapleu et leur minéralisation en Ni-Cu-EGP: un dyke nourricier du complexe lité Yacouba ; craton Archéen de Man, Ouest Côte d'Ivoire. – Thèse PhD en co-tutelle Univ. Franche Comté-Besançon / Univ. F.H. Boigny Abidjan. Soutenance Octobre 2014, 250 p.

HOFMAN A.W. (1988). – Chemical differentiation of the Earth: the relationship between mantle, continental crust, and oceanic crust. – *Earth Planet. Sci. Lett.*, **90**, 297-314.

JACKSON S.E., PEARSON N.J., GRIFFIN W.L. & BELOUSOVA E.A. (2004). – The application of laser ablation-inductively coupled plasma-mass spectrometry to in situ U-Pb zircon geochronology. – *Chem. Geol.,* **211**, 47-69.

JEBRAK M. & MARCOUX E. (2008). – Géologie des ressources minérales. – Gouvernement du Québec, ISBN 9782551237371, 667 p.

KOUAMELAN A.N. (1996). – Géochronologie et géochimie des formations archéennes et protérozoïques de la dorsale de Man en Côte d'Ivoire, implication pour la transition Archéen-Protérozoïque. – Thèse de doctorat de l'université Géosciences-Rennes 1, France, 167 p.

KOUAMELAN A.N., PEUCAT J.J. & DELOR C. (1997). – Reliques archéennes (3.15 Ga) au sein du magmatique birimien (2.1 G.a) de Côte d'Ivoire, craton ouest-africain. – *C. R. Acad. Sci.,* Paris, **324**, IIa, 719-727.

LAMBERT D.D., FOSTER J.G., FRICK L.R., LI C. & NALDRETT A.J. (1999). – Re-Os isotopic systematics of the Voisey's bay Ni-Cu-Co magmatic ore system, Labrador, Canada. – *Lithos,* **47,** 69-88.

LEHMANN J., ARNDT N.T., WINLEY B., ZHOU M.-F., WANG C.Y. & HARRIS C. (2007). – Field relationships and geochemical constraints on the emplacement of the Jinchuan intrusion and its Ni-Cu-PGE sulfide deposit, Gansu, China. – *Econ. Geol.,* **102,** 75-94.

LI X.H., SU L., CHUNG S., LI Z.X., LIU Y., SONG B. & LIU D.Y. (2005). – Formation of the Jinchuan ultramafic intrusion and the world's third largest Ni-Cu sulfide deposit: Associated with the ~825 Ma south China mantle plume? – *Geochem. Geophys. Geosyst.,* **6** (11), Q11004.

LOMPO M. (2009). – Geodynamic evolution of the 2.25-2.0 Ga Palaeoproterozoic magmatic rocks in the Man-Leo shield of the West African craton. A model of subsidence of an oceanic plateau. *In:* S.M. REDDY, R. MAZUMDER, D.A.D. EVANS and A.S. COLLINS, Eds, Paleoproterozoic supercontinents and global evolution. – *Geol. Soc. London*, Sp. Publ., **323**, 231-254.

LOMPO M. (2010). – Paleoproterozoic structural evolution of the Man-Leo shield (West Africa). Key structures for vertical to transcurrent tectonics. – *J. Afr. Earth Sci.,* **58,** 19-36.

LUDWIG K.R. (2001). – User manual for Isoplot/Ex rev. 2.49. A geochronological toolkit for Microsoft Excel. 1a, 56 p.

MAIER W.D., BARNES S.J., ARINDAM S., RIPLEY E., CHUSI LI & LIVESEY T. (2010). – The Kabanga Ni sulfide deposit, Tanzania: I. Geology, petrography, silicate rock geochemistry, and sulfur and oxygen isotopes. – *Miner. Deposita,* doi: 10.1007/s00126-010-0280-0.

MÜLLER W., SHELLEY M., MILLER P. & BROUDE S. (2009). – Initial performance metrics of a new custom-designed ArF excimer LA-ICPMS system coupled to a two-volume laser-ablation cell. – *J. Anal. At. Spectrom.*, **24**, 209-214.

NALDRETT A.J. (1989). – Magmatic sulfide deposits. – Oxford Union Press, Oxford, 196 p.

NALDRETT A.J. (2004). – Magmatics sulfide deposits: Geology, geochemistry and exploration: Heidelberg. – Springer Verlag, Heidelberg, 728 p.

OUATTARA N. (1998). – Pétrologie, géochimie et métallogénie des sulfures du groupe du platine des ultrabasites de Côte d'Ivoire: Signification géodynamique et implications sur les processus de croissance crustale à l'archéen et au paléoprotérozoïque. – Thèse de doctorat de l'université d'Orléans France, 199 p.

PITRA P., KOUAMELAN A.N., BALLÈVRE M. & PEUCAT J.J. (2010). – Palaeo-Proterozoic high-pressure granulite overprint of the Archean continental crust: evidence for homogeneous crustal thickening (Man rise, Ivory Coast). – *J. Metam. Geol.*, **28**, 41-58.

PRONOST J. (2005). – Effets de la contamination continentale et des interactions fluides-roches sur le platreef, complexe igné du Bushveld, Afrique du Sud. – Thèse de doctorat de l'université de Clermont-Ferrand II-Blaise Pascal (France), 258 p.

ROEDER P.L & EMSLIE R.F. (1970). – Olivine-liquid equilibrium. – *Contrib. Mineral. Pet.,* **29**, 275-89.

SHIBO LI & HALL C. (1993). – Petrography and paragenesis of platinium-group mineral in Jinchuan ultramafic intrusion, northwest China. – *Trans. Instn Min. Metall (Sect. B*: *Appl. Earth sci.*), **102**, 164-180.

SONG X., WANG Y. & CHEN L. (2011). – Magmatic Ni-Cu-(PGE) deposits in magma plumbing systems: Features, formation and exploration. – *Geosci. Front.,* **2(3)**, 375-384.

THIEBLEMONT D., GOUJOU J.C., EGAL E., COCHERIE A., DELOR C., LAFON J.M. & FANNING C.M. (2004). – Archaean evolution of the Leo rise and its Eburnean reworking. – *J. Afr. Earth Sci*., **39**, 97-104.

THOMSON R.N., MORRISON M.A., DICKIN A.P. & HENDRY G.L. (1983). – Continental flood basalts... arachnids rule OK? *In*: C.J. HAWKESWORTH and M.J. NORRY, Eds., Continental basalts and mantle xenoliths. – Shiva Publishing Ltd, Nantwich, 158-185.

VAN ACHTERBERGH E, RYAN C.G., JACKSON S.E. & GRIFFIN W. (2001). **–** Data reduction software for LA-ICP-MS. *In*: P. SYLVESTER, Ed., Laser ablation-ICPMS in the earth science. **–** *Mineral. Assoc. Canada,* **29**, 239-243.

VOSHAGE H., HOFMANN A.W., MAZZUCCHELLI M., RIVALENTI G., SINIGOI S., RACZEK I. & DEMARCHI G. (1990). – Isotopic evidence from the Ivrea zone for a hybrid lower crust formed by magmatic underplating. – *Nature,* **347**, 731-736.

YANG X.Z., ISHIHARA S. & ZHAO D.H. (2006). – Genesis of the Jinchuan PGE deposit, China: evidence from fluid inclusions, mineralogy and geochemistry of precious elements. – *Mineral. Petrol.,* **86**, 109-128.

http://www.samaresources.com/s/Samapleu.asp: official site for the Sama Nickel-CI